International Journal of Heat and Fluid Flow 000 (2016) 1–17

Contents lists available at ScienceDirect

International Journal of Heat and Fluid Flow

journal homepage: www.elsevier.com/locate/ijhff

Effects of temperature-dependent contact angle on the flow dynamics of an impinging droplet on a hot solid substrate

Jagannath Venkatesan, Sangeetha Rajasekaran, Anubhav Das, Sashikumaar Ganesan*

Department of Computational and Data Sciences, Indian Institute of Science, Bangalore-560012, India

ARTICLE INFO

Article history:
Available online xxx

Keywords:
Dynamic contact angle
Impinging droplet
Heat transfer
Marangoni convection
Finite elements
ALE approach

ABSTRACT

A temperature-dependent dynamic contact angle as a function of temperature-dependent surface tension and reference equilibrium contact angle is proposed for modeling of moving contact line flows, in particular, for computations of liquid droplet impingement on a hot solid substrate. The fluid flow in the liquid droplet is described by the time-dependent incompressible Navier–Stokes equations, whereas the heat transfer in the liquid droplet and in the solid substrate is described by the energy equation. The arbitrary Lagrangian–Eulerian (ALE) approach together with the finite element method is used to solve the governing equations in a time-dependent domain. Further, the Marangoni effects are incorporated into the model without evaluating the tangential derivatives of the temperature on the free surface. The effects of temperature-dependent contact angle on the flow dynamics of the droplet and on the heat transfer from the solid substrate into the liquid droplet are studied for different Reynolds numbers, Weber numbers, solid phase Peclet numbers, solid phase initial temperatures and reference equilibrium contact angles. Numerical studies show that the influence of the temperature-dependent contact angle is negligible in partially wetting droplets, whereas the effects on the wetting diameter and on the total heat transfer are 10.79% and 7.36% respectively in the considered highly wetting and non–wetting droplets.

1. Introduction

Understanding the physics involved in cooling and/or temperature regulations of solid substrates using sprays are of fundamental importance in a wide variety of industrial applications such as fuel injection, thin film coating, spray cooling, internal combustion engines, micro/nano material fabrication, etc. Most of these applications involve heat transfer and their computations are of particular scientific interest. Modeling of the heat transfer mechanism involved in the process of a liquid droplet impinging on a hot solid substrate is very complex. Tracking/capturing the moving boundaries and incorporating the dynamic contact angle are the main challenges in the modeling. Further, an accurate approximation of the curvature, precise inclusion of the Marangoni and surface forces and handling the jumps in the liquid and solid material parameters make the computations more challenging.

Apart from all these challenges, handling the moving contact line is one of the main challenges in moving contact line flows (Ganesan, 2013; Ren and Weinan E, 2007; Sui et al., 2014). The choice of an appropriate boundary condition on the liquid-solid interface and a dynamic contact angle are the two challenges associated with the modeling of moving contact line flows. The use of the classical no-slip boundary condition on the liquid-solid interface induces an unbounded stress singularity at the moving contact line, where the liquid, solid and gas phases intersect. Several approaches have been proposed in the literature to alleviate this singularity, see for example, Behr and Abraham (2002); Eggers and Stone (2004); Hocking (1977). Among all, the Navier-slip boundary condition has been widely accepted to ease the singularity at the moving contact line. Nevertheless, the main challenge in using the Navier-slip boundary condition is the choice of the slip coefficient. The slip coefficient is often determined by comparing computationally obtained wetting diameter with experimental results (Ganesan, 2013; Ganesan et al., 2014). A number of expressions have been proposed for the slip coefficient, see for example, Cox (1986); Dussan V (1976); Hocking (1977) for different moving contact line problems. Recently, a mesh-dependent slip relation for impinging droplets has been proposed in Venkatesan and Ganesan (2015), and we use it in this work.

The contact angle is an important property of a liquid droplet that is determined by the interfacial tensions between the liquid, solid and gas phases. It deviates from its thermodynamic equilibrium value when the droplet spreads and recoils. In addition,

* Corresponding author.
E-mail addresses: jagan@cmg.cds.iisc.ac.in (J. Venkatesan), sangeetha@cmg.cds.iisc.ac.in (S. Rajasekaran), anubhav@cmg.cds.iisc.ac.in (A. Das), sashi@cds.iisc.ac.in (S. Ganesan).

http://dx.doi.org/10.1016/j.ijheatfluidflow.2016.10.003
0142-727X/

Nomenclature

α_F	convection heat transfer coefficient on liquid-gas interface
β_ϵ	slip number
Γ_F	free surface
Γ_N	non-wetting part of the solid phase
Γ_S	liquid–solid interface
$\hat{\gamma}$	surface tension factor
δt	time step length
ζ	contact line
θ_d	dynamic contact angle
θ_e^{ref}	reference equilibrium contact angle
$\mathcal{K}$	curvature
λ_F	thermal conductivity of fluid
λ_S	thermal conductivity of solid
μ	dynamic viscosity of fluid
ν_F	unit outward normal vector on free surface
ν_S	unit outward normal vector on liquid–solid interface
$\boldsymbol{\nu}_\zeta$	co–normal vector at the contact line
ρ	density of fluid
ρ_S	density of solid
σ	liquid–gas surface tension
σ^{sg}	solid–gas surface tension
σ^{sl}	solid–liquid surface tension
σ_{ref}	reference surface tension
τ_F	unit tangential vector on free surface
τ_S	unit tangential vector on liquid–solid interface
Ω	computational domain for energy equation
Ω_F	fluid domain
Ω_S	solid domain
$\mathbb{D}$	deformation tensor of fluid velocity
$\mathbb{I}$	identity tensor
$\mathbb{S}$	stress tensor of fluid
∇_Γ	tangential gradient operator on the free surface
$\otimes$	tensor product
id_Γ	identity mapping
$\mathcal{C}_1$	negative rate of change of surface tension with temperature
tr	trace
Bi	Biot number
Fr	Froude number
Pe_F	fluid Peclet number
Pe_S	solid Peclet number
Re	Reynolds number
We	Weber number
c_p^F	specific heat of fluid
c_p^S	specific heat of solid
T_∞	temperature in surrounding gas
T_F	temperature in fluid
T_G	temperature at solid–gas interface
T_{ref}	reference temperature
T_S	temperature in solid
d_0	initial droplet diameter
d/d_0	dimensionless wetting diameter
u_{imp}	impact speed of droplet
g	gravitational constant
p	pressure
q	pressure space test function
t	time
I	given end time
L	characteristic length
Q	pressure space
U	characteristic velocity
V	velocity space
e	unit vector in the direction opposite to gravitational force
n	unit outward normal on non-wetting part of solid phase
u	fluid velocity
v	Velocity space test function
w	domain velocity

several experimental studies on the influence of the temperature on the contact angle have been reported in the literature, see for example, Adamson (1973); Bernardin et al. (1997); Chandra et al. (1996); Neumann (1974); Neumann et al. (1971); Petke and Ray (1969); de Ruijter et al. (1998); Schonhorn (1966); Steinke (2001). For instance, two distinct temperature regimes for the static advancing contact angle of water on an aluminium surface have been observed in Bernardin et al. (1997). A relatively constant contact angle of 90° has been observed for temperatures less than 120°C, whereas a fairly linear decrease in the contact angle is observed for temperatures above 120°C. Next, the influence of the temperature on contact angles at low temperatures ($5^\circ - 100^\circ$ C) has been investigated in Adamson (1973); Neumann (1974); Neumann et al. (1971). It has been reported in these studies that $|\partial\theta/\partial T| \approx 0.1\text{deg K}^{-1}$. Further, the influence of the temperature on the contact angle for water and several other liquids on six polymeric solids has been studied in Petke and Ray (1969). The authors have found that the value of $|\partial\theta/\partial T|$ varies between 0.03 deg K^{-1} and 0.18 deg K^{-1} for the temperature range $5^\circ - 100^\circ$ C. Since the flow dynamics of the droplet directly depends on the contact angle, it is essential to use a temperature-dependent dynamic contact angle model to accurately capture the flow dynamics during the spreading and recoiling.

A considerable number of numerical studies for a liquid droplet impinging on a hot solid surface using the Volume–of–fluid method have been reported in the literature (Briones et al., 2010; Ghafouri-Azar et al., 2003; Harvie and Fletcher, 2001; Putnam et al., 2012; Strotos et al., 2008). Numerical studies using the Level set method (Y. Ge, 2005; 2006), the Immersed Boundary method (Francois and Shyy, 2003a; 2003b) and the Lagrangian method (Z. Zhao, 1996) have also been reported in the literature. Further, computations using the ALE approach for a liquid droplet impinging on a hot solid substrate have been presented in Ganesan et al. (2014); 2015). In all these numerical studies the contact angle, which is independent of temperature, have been considered. Recently, a dynamic contact angle model that depends on surfactants has been proposed in Ganesan (2015); M.-C. Lai and Huang (2010). However, to the best of the authors' knowledge, a temperature-dependent dynamic contact angle for computations of droplet impingement on a hot solid substrate has not been used in the literature.

In this paper, a temperature-dependent dynamic contact angle using the Young's law which is a function of temperature-dependent surface tension and reference equilibrium contact angle is proposed. Further, the effects of temperature-dependent dynamic contact angle on the flow dynamics of the droplet are studied by comparing the results with temperature-independent contact angle model (Ganesan et al., 2014; 2015). We use the sharp interface ALE finite element approach for computations of a non-isothermal liquid droplet impinging on a hot solid substrate. The inclusion of the contact angle is straightforward in interface resolved numerical schemes and explained in Ganesan et al. (2014). However, the choice of an appropriate contact angle in

Please cite this article as: J. Venkatesan et al., Effects of temperature-dependent contact angle on the flow dynamics of an impinging droplet on a hot solid substrate, International Journal of Heat and Fluid Flow (2016), http://dx.doi.org/10.1016/j.ijheatfluidflow.2016.10.003

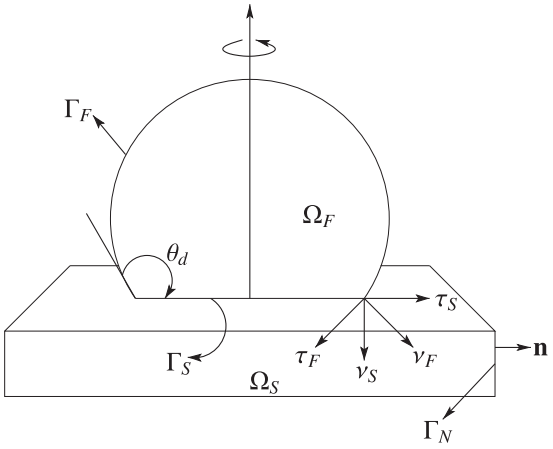

Fig. 1. Model of an impinging droplet on a hot solid substrate.

computations is very challenging, and the choice of the equilibrium values for shape interface schemes has been proposed in Ganesan (2013). Further, the Marangoni convection is included in the variational form of the Navier–Stokes equations without evaluating the tangential derivatives of the surface tension.

The paper is organized as follows. Section 2 presents an overview of the model, the governing equations for the fluid flow and the heat transfer in the liquid and solid phases and the contact angle models. Section 3 presents a brief overview of the numerical scheme used, in particular, the weak form of the governing equations, finite element discretization and the ALE approach. Section 4 is concerned with the parametric study for different Reynolds numbers, Weber numbers, Peclet numbers, solid phase initial temperatures and equilibrium contact angles demonstrating the effect of temperature-dependent contact angle on the flow dynamics of the droplet and on the heat transfer from the solid substrate into the liquid droplet. Finally, a summary based on our observations is provided in Section 5.

2. Mathematical model

2.1. Model problem

A non–isothermal liquid droplet impinging on a hot solid substrate is considered. The computation starts when the droplet comes into contact with the solid substrate, and continued for a prescribed time or until the droplet attains its equilibrium state. Fig. 1 shows the schematic representation of the computational model. Here, Ω_F and Ω_S represent the fluid and solid domains, Γ_S and Γ_F represent the liquid-solid and the liquid-gas (free surface) interfaces, respectively. Further, τ_F and ν_F are the unit tangential and unit outward normal vectors on Γ_F and τ_S and ν_S are the unit tangential and unit outward normal vectors on Γ_S. Moreover, θ_d is the dynamic contact angle of the droplet, Γ_N is the non-wetting part of the solid and $\mathbf{n}$ is the unit outward normal vector on Γ_N.

2.2. Governing equations

Let $\Omega_F \subset \mathbb{R}^3$ and $\Omega_S \subset \mathbb{R}^3$ be the fluid and solid domains, respectively. We assume that the liquid is incompressible and the material properties (density, viscosity, thermal conductivity and specific heat) are constants in both the liquid and solid substrate. In addition, we assume that there is no rapid evaporation or Leidenfrost phenomenon. The fluid flow in the liquid droplet is described by the time-dependent incompressible Navier-Stokes equations and the heat transfer in the moving droplet and in the solid substrate is described by the energy equation. Detailed description of the mathematical model and the numerical scheme used in this paper have been presented in Ganesan et al. (2014), whereas a brief description of the model and the numerical scheme are presented here. Let

$$x = \frac{\tilde{x}}{L}, \quad \mathbf{u} = \frac{\tilde{\mathbf{u}}}{U}, \quad \mathbf{w} = \frac{\tilde{\mathbf{w}}}{U}, \quad t = \frac{\tilde{t}U}{L},$$
$$\mathrm{I} = \frac{\tilde{\mathrm{I}}U}{L}, \quad p = \frac{\tilde{p}}{\rho U^2}, \quad \mathrm{T} = \frac{\tilde{\mathrm{T}} - \mathrm{T}_\infty}{\mathrm{T}_{ref} - \mathrm{T}_\infty}$$

be the dimensionless length x, fluid velocity $\mathbf{u}$, domain velocity $\mathbf{w}$, time t, given end time I, pressure p and temperature T, respectively. Moreover, the tilde over the variables indicate its dimensional form. Here, L and U are characteristic length and velocity scales, ρ the density of the fluid, T_∞ the temperature of the surrounding gas and T_{ref} is a given reference temperature at which the surface tension is σ_{ref}, that satisfies the relation for the surface tension

$$\sigma(\tilde{\mathrm{T}}_F) = \sigma_{ref} - \mathcal{C}_1(\tilde{\mathrm{T}}_F - \mathrm{T}_{ref}).$$

Here, $\tilde{\mathrm{T}}_F$ is the dimensional temperature on the free surface and $\mathcal{C}_1 > 0$ is the negative rate of change of surface tension with respect to the temperature. Further, we define the dimensionless numbers (Reynolds, Weber, Froude and slip, respectively)

$$\mathrm{Re} = \frac{\rho U L}{\mu}, \quad \mathrm{We} = \frac{\rho U^2 L}{\sigma_{ref}}, \quad \mathrm{Fr} = \frac{U^2}{Lg}, \quad \beta_\epsilon = \frac{1}{\epsilon_\mu \rho U},$$

where μ is the viscosity of the fluid, g is the acceleration due to gravity and ϵ_μ is the slip coefficient in the Navier-slip with friction boundary condition.

The flow dynamics in the scaled domain is then described by the dimensionless time-dependent incompressible Navier-Stokes equations

$$\frac{\partial \mathbf{u}}{\partial t} + (\mathbf{u}\cdot\nabla)\mathbf{u} - \nabla\cdot\mathbb{S}(\mathbf{u},p) = \frac{1}{\mathrm{Fr}}\mathbf{e} \quad \text{in } \Omega_F(t)\times(0,\mathrm{I}), \tag{1}$$

$$\nabla\cdot\mathbf{u} = 0 \quad \text{in } \Omega_F(t)\times(0,\mathrm{I}), \tag{2}$$

where (1) is the momentum balance equation and (2) is the mass balance equation for the fluid. Here, $\mathbf{e}$ is the unit vector in the direction opposite to the gravitational force. The dimensionless stress tensor $\mathbb{S}(\mathbf{u},p)$ and the deformation tensor $\mathbb{D}(\mathbf{u})$ for the incompressible Newtonian fluid are given by

$$\mathbb{S}(\mathbf{u},p) = \frac{2}{\mathrm{Re}}\mathbb{D}(\mathbf{u}) - p\mathbb{I}, \quad \mathbb{D}(\mathbf{u}) = \frac{1}{2}\left(\nabla\mathbf{u} + \nabla\mathbf{u}^{\mathrm{T}}\right).$$

Here, $\mathbb{I}$ is the identity tensor. The Navier-Stokes equations are closed with the initial and boundary conditions. At time $t=0$, we assume that the droplet is of spherical shape with diameter d_0 and the initial condition

$$\mathbf{u}(\cdot,0) = \mathbf{u}_0/U,$$

where $\mathbf{u}_0 = (0,0,-u_{imp})$, is the initial velocity and u_{imp} is the impinging speed of the droplet. On the liquid-solid interface, the Navier–slip boundary condition

$$\begin{aligned} \mathbf{u}\cdot\nu_S &= 0 && \text{on} \quad \Gamma_S(t)\times(0,I) \\ \tau_S\cdot\mathbb{S}(\mathbf{u},p)\cdot\nu_S &= -\beta_\epsilon\mathbf{u}\cdot\tau_S && \text{on} \quad \Gamma_S(t)\times(0,I) \end{aligned} \tag{3}$$

is imposed. The first condition is the no penetration boundary condition, i.e., the fluid cannot penetrate an impermeable solid and thus the normal component of the fluid velocity is zero. The second condition is the slip with friction boundary condition, i.e., on the liquid-solid interface, the tangential stress is proportional to tangential velocity of the fluid. On the free surface, the kinematic boundary condition

$$\mathbf{u}\cdot\nu_F = \mathbf{w}\cdot\nu_F \quad \text{on } \Gamma_F(t)\times(0,I)$$

Please cite this article as: J. Venkatesan et al., Effects of temperature-dependent contact angle on the flow dynamics of an impinging droplet on a hot solid substrate, International Journal of Heat and Fluid Flow (2016), http://dx.doi.org/10.1016/j.ijheatfluidflow.2016.10.003

holds, i.e., the normal component of the fluid velocity on the free surface is equal to the normal component of free surface velocity. Further, the force balancing condition

$$\mathbb{S}(u,p)\cdot\nu_F = \frac{1}{\mathrm{We}}\nabla_\Gamma\cdot\left(\hat{\gamma}\,\nabla_\Gamma id_\Gamma\right) \quad \text{on} \quad \Gamma_F(t)\times(0,\mathrm{I}) \tag{4}$$

is imposed. Note that

$$\nabla_\Gamma\cdot\left(\hat{\gamma}\,\nabla_\Gamma id_\Gamma\right) = \nabla_\Gamma\hat{\gamma} - \hat{\gamma}\,\mathcal{K}\nu_1,$$

where $\mathcal{K}$ is the sum of the principle curvatures, see Ganesan (2015) for the derivation of the above relation. Using the relation (4) instead of the standard relation, the calculation of $\nabla_\Gamma\hat{\gamma}$ and the handling of the curvature $\mathcal{K}$ are avoided (Ganesan et al., 2015). Here, id_Γ is an identity mapping and ∇_Γ is the tangential gradient operator on the free surface. For instance, the tangential gradient of a scalar field ϕ and the tangential divergence of a vector field $\mathbf{v}$ are defined by

$$\nabla_\Gamma\phi = (\mathbb{I}-\nu_F\otimes\nu_F)\phi, \qquad \nabla_\Gamma\cdot\mathbf{v} = \mathrm{tr}\ (\nabla_\Gamma\mathbf{v}).$$

Here, $\otimes$ and tr refer to the tensor product and trace respectively. The dimensionless form of the temperature-dependent surface tension which induces the Marangoni convection is given by

$$\sigma(\mathrm{T}_F) = \sigma_{ref}\hat{\gamma}(\mathrm{T}_F), \quad \hat{\gamma}(\mathrm{T}_F) = 1 - \frac{\mathcal{C}_1}{\sigma_{ref}}(\mathrm{T}_F - 1). \tag{5}$$

Next, the temperature distribution in the liquid droplet and in the solid substrate is described by the dimensionless energy equations

$$\frac{\partial \mathrm{T}_F}{\partial t} + \mathbf{u}\cdot\nabla\mathrm{T}_F - \frac{1}{\mathrm{Pe}_F}\Delta\mathrm{T}_F = 0 \qquad \text{in } \Omega_F(t)\times(0,\mathrm{I}), \tag{6}$$

$$\frac{\partial \mathrm{T}_S}{\partial t} - \frac{1}{\mathrm{Pe}_S}\Delta\mathrm{T}_S = 0 \qquad \text{in } \Omega_S(t)\times(0,\mathrm{I}), \tag{7}$$

with the initial conditions

$$\mathrm{T}_F(x,0) = \frac{\mathrm{T}_{F,0}-\mathrm{T}_\infty}{\mathrm{T}_{ref}-\mathrm{T}_\infty} \quad \text{in} \quad \Omega_F(0),$$

$$\mathrm{T}_S(x,0) = \frac{\mathrm{T}_{S,0}-\mathrm{T}_\infty}{\mathrm{T}_{ref}-\mathrm{T}_\infty} \quad \text{in} \quad \Omega_S(0).$$

Here, $\mathrm{T}_{F,0}$ and $\mathrm{T}_{S,0}$ denote the initial temperatures in the fluid and solid phases, respectively. The boundary condition for the temperature on the free surface is given by

$$-\frac{\partial \mathrm{T}_F}{\partial \nu_F} = \mathrm{Bi}\ \mathrm{T}_F \quad \text{on } \Gamma_F(t)\times(0,\mathrm{I}). \tag{8}$$

On the liquid-solid interface, the temperature and heat flux are assumed to be continuous, and we impose the transition conditions

$$\mathrm{T}_F = \mathrm{T}_S, \quad \frac{\partial \mathrm{T}_F}{\partial \nu_F} = -\frac{\lambda_S}{\lambda_F}\frac{\partial \mathrm{T}_S}{\partial \nu_S} \qquad \text{on } \Gamma_S(t)\times(0,\mathrm{I}). \tag{9}$$

On $\Gamma_N(t)$, we impose the adiabatic boundary condition

$$\frac{\partial \mathrm{T}_S}{\partial \mathbf{n}} = 0 \qquad \text{on } \Gamma_N(t)\times(0,\mathrm{I}). \tag{10}$$

Further, the dimensionless (fluid Peclet, solid Peclet and Biot) numbers are given by

$$\mathrm{Pe}_F = \frac{LUc_p^F\rho}{\lambda_F}, \quad \mathrm{Pe}_S = \frac{LUc_p^S\rho_S}{\lambda_S}, \quad \mathrm{Bi} = \frac{\alpha_F L}{\lambda_F},$$

where λ_F, λ_S the thermal conductivities, ρ, ρ_S the densities, c_p^F, c_p^S the specific heat of the fluid and the solid phases. Further, α_F is the convection heat transfer coefficient on the free surface.

2.3. Temperature–dependent equilibrium contact angle

In thermodynamic equilibrium state, the contact angle is related to the interfacial tensions of the free surface σ, solid-liquid σ^{sl} and the solid-gas σ^{sg} through the Young's equation

$$\cos(\theta) = \frac{\sigma^{sg}-\sigma^{sl}}{\sigma}. \tag{11}$$

In general, the contact angle θ in the Young's Eq. (11) is referred to as static or equilibrium contact angle. At the equilibrium state, the equilibrium contact angle is unique for the considered gas, liquid and solid material phases. However, the contact angle deviates from the equilibrium values when the contact line moves, and the difference between the advancing and receding contact angles is referred to as the *contact angle hysteresis*. The contact angle that incorporated this hysteresis behaviour is called the dynamic contact angle.

The choice of a contact angle in computations is itself a topic of research, and several contact angle models incorporating the contact line velocity are proposed in the literature, see Ganesan (2013) for a comparative study of different models. Two contact angle models, one with independent of temperature and another as a function of temperature, are considered in this study. During the droplet deformation, the dynamic contact angle deviates from the equilibrium value. It induces an unbalanced Young force (Gennes, 1985),

$$\mathrm{F}_Y = \sigma_{ref}^{sg} - \sigma_{ref}^{sl} - \sigma_{ref}\cos\theta_d = \sigma_{ref}(\cos\theta_e^{ref} - \cos\theta_d),$$

at the contact line since $\theta_d \neq \theta_e^{ref}$. Thus we have

$$\sigma_{ref}\cos\theta_e^{ref} = \sigma_{ref}\cos\theta_d + \mathrm{F}_Y.$$

Here, θ_e^{ref} is the equilibrium contact angle of the droplet for the given reference temperature T_{ref}. At the equilibrium position, the unbalanced Young's force has to be zero, and hence we impose $\mathrm{F}_Y = 0$ in the model. It results in

$$\text{M1:} \qquad \theta_d = \theta_e^{ref}, \tag{12}$$

which is independent of the temperature. The choice of equilibrium value in computations does not mean that the dynamic contact angle is fixed to the equilibrium value during the computations. Nevertheless, the surface force at the contact line becomes unbalanced due to the imposed condition $\mathrm{F}_Y = 0$, and it gets translated into kinetic energy that induces the slip velocity. Consequently, the slip velocity drives the contact line into the equilibrium position, eventually, the dynamic contact angle attains the prescribed equilibrium value at the equilibrium position. Thus, it is necessary to allow the liquid to slip in the vicinity of the contact line, and it is another justification for the choice of Navier–slip boundary condition on the liquid-solid interface.

In thermodynamic equilibrium state, the Young's Eq. (11) holds true. However, a nonuniform distribution of temperature on the interfaces induces an unbalanced force

$$\mathrm{F}_Y = \sigma^{sg}(\mathrm{T}_G) - \sigma^{sl}(\mathrm{T}_S) - \sigma(\mathrm{T}_F)\cos\theta_d,$$

where T_G is the temperature on the solid-gas interface. Imposing the zero unbalanced force, $F_Y = 0$, as before, results in the temperature-dependent dynamic contact angle

$$\theta_d = \cos^{-1}\left(\frac{\sigma^{sg}(\mathrm{T}_G) - \sigma^{sl}(\mathrm{T}_S)}{\sigma(\mathrm{T}_F)}\right).$$

Since $\sigma^{sg}(\mathrm{T}_G)$ and $\sigma^{sl}(\mathrm{T}_S)$ are seldom available, the above relation cannot be used in computations. Nevertheless, on the application of the relation (5) with the assumption that the rate of change of

Please cite this article as: J. Venkatesan et al., Effects of temperature-dependent contact angle on the flow dynamics of an impinging droplet on a hot solid substrate, International Journal of Heat and Fluid Flow (2016), http://dx.doi.org/10.1016/j.ijheatfluidflow.2016.10.003

both $\sigma^{sg}(T_G)$ and $\sigma^{sl}(T_S)$ with respect to the temperature are same and $T_F = T_G = T_S$ at the contact line, we get

$$\text{M2:}\quad \theta_d(T_F) = \cos^{-1}\left(\frac{\cos\theta_e^{ref}}{\hat{\gamma}(T_F)}\right). \tag{13}$$

Suppose $\tilde{T}_F < T_{ref}$, then $\hat{\gamma}(T_F) > 1$. Hence, the dynamic contact angle, θ_d, increases with temperature for wetting droplets ($\theta_e^{ref} < 90^\circ$), and decreases with temperature for non-wetting droplets ($\theta_e^{ref} > 90^\circ$). Conversely, if $\tilde{T}_F > T_{ref}$, then $\hat{\gamma}(T_F) < 1$ and hence, the dynamic contact angle decreases with temperature for wetting droplets and increases for non-wetting droplets. It can also be noted that the temperature has no effect on the dynamic contact angle when $\theta_e^{ref} = 90^\circ$.

3. Numerical scheme

The finite element scheme using the ALE approach proposed in Ganesan et al. (2014) is used in this work with different contact angle models. We recall the key parts in the numerical scheme, whereas the reader is referred to Ganesan et al. (2014) for a detailed description of the numerical scheme.

3.1. Weak formulation

Let $L^2(\Omega(t))$, $H^1(\Omega(t))$ and $(\cdot,\cdot)_{\Omega(t)}$ be the standard Sobolev spaces and the inner product in $L^2(\Omega(t))$ and its vector-valued versions, respectively. Further, we define the velocity and pressure spaces as

$$V := \left\{\mathbf{v} \in H^1(\Omega_F(t))^3 : \mathbf{v}\cdot\nu_S = 0 \text{ on } \Gamma_S(t)\right\},$$
$$Q := L^2(\Omega_F(t)).$$

Here, the velocity space is chosen in such a way that the no penetration boundary condition $\mathbf{u}\cdot\nu_S = 0$ on the liquid-solid interface $\Gamma_S(t)$ is incorporated in both the ansatz and test spaces. Now we multiply the momentum (1) and mass balance Eq. (2) by test functions $\mathbf{v} \in V$ and $q \in Q$, respectively, and integrate over $\Omega_F(t)$. By applying the Gaussian theorem for the stress tensor, we get

$$-\int_{\Omega_F(t)} \nabla\cdot\mathbb{S}(\mathbf{u},p)\cdot\mathbf{v}\,dx + \int_{\partial\Omega_F(t)} \mathbf{v}\cdot\mathbb{S}(\mathbf{u},p)\cdot\nu\,d\gamma = \frac{2}{\mathrm{Re}}\int_{\Omega_F(t)} \mathbb{D}(\mathbf{u}):\mathbb{D}(\mathbf{v})\,dx - \int_{\Omega_F(t)} p\nabla\cdot\mathbf{v}\,dx.$$

We now split the boundary integral into integrals over $\Gamma_S(t)$ and $\Gamma_F(t)$ as

$$\int_{\partial\Omega_F(t)} \mathbf{v}\cdot\mathbb{S}(\mathbf{u},p)\cdot\nu\,d\gamma = \int_{\Gamma_S(t)} \mathbf{v}\cdot\mathbb{S}(\mathbf{u},p)\cdot\nu_S\,d\gamma_S + \int_{\Gamma_F(t)} \mathbf{v}\cdot\mathbb{S}(\mathbf{u},p)\cdot\nu_F\,d\gamma_F.$$

Then using the orthonormal decomposition

$$\mathbf{v} = (\mathbf{v}\cdot\nu_S)\nu_S + \sum_{i=1}^{2}(\mathbf{v}\cdot\tau_{i,S})\tau_{i,S} \quad \text{on } \Gamma_S, \tag{14}$$

and using the Navier-slip boundary condition (3), the integral over liquid-solid interface $\Gamma_S(t)$ becomes

$$\int_{\Gamma_S(t)} \mathbf{v}\cdot\mathbb{S}(\mathbf{u},p)\cdot\nu_S\,d\gamma_S = -\beta_\epsilon\sum_{i=1}^{2}\int_{\Gamma_S(t)} (\mathbf{u}\cdot\tau_{i,S})(\mathbf{v}\cdot\tau_{i,S})\,d\gamma_S.$$

Similarly, after applying the force balancing condition (4), the integral over the free surface $\Gamma_F(t)$ becomes

$$\int_{\Gamma_F(t)} \mathbf{v}\cdot\mathbb{S}(\mathbf{u},p)\cdot\nu_F\,d\gamma_F = -\frac{1}{\mathrm{We}}\int_{\Gamma_F(t)} \hat{\gamma}(T_F)\nabla_\Gamma id_\Gamma : \nabla_\Gamma\mathbf{v}\,d\gamma_F + \frac{1}{\mathrm{We}}\int_{\zeta(t)} \hat{\gamma}(T_F)\nu_\zeta\cdot\mathbf{v}\,d\zeta. \tag{15}$$

Here, $\zeta(t)$ is the contact line and $\boldsymbol{\nu}_\zeta$ is the co–normal vector at the contact line. In the second term of Eq. (15), we decompose the test function as in (14) and use the fact that $\mathbf{v}\cdot\nu_S = 0$ on $\Gamma_S(t)$, to get

$$\frac{1}{\mathrm{We}}\int_{\zeta(t)} \hat{\gamma}(T_F)\nu_\zeta\cdot\mathbf{v}\,d\zeta = \frac{1}{\mathrm{We}}\int_{\zeta(t)} \hat{\gamma}(T_F)(\nu_\zeta\cdot\tau_{i,S})(\mathbf{v}\cdot\tau_{i,S})\,d\zeta = \frac{1}{\mathrm{We}}\int_{\zeta(t)} \hat{\gamma}(T_F)\cos(\theta_d)(\mathbf{v}\cdot\tau_{i,S})\,d\zeta.$$

In the above derivation, we used the relation $\nu_\zeta\cdot\tau_{i,S} = \cos(\theta_d)$. This technique of inclusion of contact angle in the integral over the contact line (Ganesan, 2015; Ganesan et al., 2015) is different from the Laplace-Beltrami operator technique used in Ganesan (2013); Ganesan et al. (2014); Ganesan and Tobiska (2008). Further, the Marangoni effects are incorporated into the numerical scheme without evaluating the tangential gradient of the surface tension (Ganesan, 2015; Ganesan et al., 2015). After imposing all the boundary conditions, the variational form of the Navier–Stokes Eqs. (1) and (2) read:

For given θ_d, $\mathbf{u}_0$ and $\Omega_F(0)$, find $(\mathbf{u}, p) \in V \times Q$ such that

$$\left(\frac{\partial\mathbf{u}}{\partial t},\mathbf{v}\right)_{\Omega_F(t)} + a(\mathbf{u};\mathbf{u},\mathbf{v}) - b(p,\mathbf{v}) + b(q,\mathbf{u}) = f(\mathbf{v}) \tag{16}$$

for all $(\mathbf{v}, q) \in V \times Q$, where

$$a(\hat{\mathbf{u}};\mathbf{u},\mathbf{v}) = \int_{\Omega_F(t)} \frac{2}{\mathrm{Re}}\mathbb{D}(\mathbf{u}):\mathbb{D}(\mathbf{v}) + (\hat{\mathbf{u}}\cdot\nabla)\mathbf{u}\cdot\mathbf{v}\,dx + \beta_\epsilon\int_{\Gamma_S(t)}\sum_{i=1}^{2}(\mathbf{u}\cdot\tau_{i,S})(\mathbf{v}\cdot\tau_{i,S})\,d\gamma_S,$$

$$b(q,\mathbf{v}) = \int_{\Omega_F(t)} q\,\nabla\cdot\mathbf{v}\,dx,$$

$$f(\mathbf{v}) = \frac{1}{\mathrm{Fr}}\int_{\Omega_F(t)} \mathbf{e}\cdot\mathbf{v}\,dx - \frac{1}{\mathrm{We}}\int_{\Gamma_F(t)} \hat{\gamma}(T_F)\nabla_\Gamma id_\Gamma : \nabla_\Gamma\mathbf{v}\,d\gamma_F + \frac{1}{\mathrm{We}}\int_{\zeta(t)} \hat{\gamma}(T_F)\cos(\theta_d)\,\mathbf{v}\cdot\tau_S\,d\zeta.$$

Using the variants of contact angle, the source term f becomes

$$f(\mathbf{v}) = \frac{1}{\mathrm{Fr}}\int_{\Omega_F} \mathbf{e}\cdot\mathbf{v}\,dx - \frac{1}{\mathrm{We}}\int_{\Gamma_F(t)} \hat{\gamma}(T_F)\nabla_\Gamma id_\Gamma : \nabla_\Gamma\mathbf{v}\,d\gamma_F + \frac{1}{\mathrm{We}}\int_{\zeta(t)} \hat{\gamma}(T_F)\cos\left(\theta_e^{ref}\right)\mathbf{v}\cdot\tau_S\,d\zeta,$$

with the M1 model (12) and becomes

$$f(\mathbf{v}) = \frac{1}{\mathrm{Fr}}\int_{\Omega_F} \mathbf{e}\cdot\mathbf{v}\,dx - \frac{1}{\mathrm{We}}\int_{\Gamma_F(t)} \hat{\gamma}(T_F)\nabla_\Gamma id_\Gamma : \nabla_\Gamma\mathbf{v}\,d\gamma_F + \frac{1}{\mathrm{We}}\int_{\zeta(t)} \cos\left(\theta_e^{ref}\right)\mathbf{v}\cdot\tau_S\,d\zeta,$$

with the M2 model (13). Note that the factor $\hat{\gamma}(T_F)$ in the contact line integral is not in the M2 model, and in both models, only the equilibrium contact angle value at the reference temperature, θ_e^{ref}, is needed in computations.

The weak form of the energy Eq. (6) is obtained by multiplying it with a test function $\psi_F \in H^1(\Omega_F(t))$. Then applying integration by parts, subsequently incorporating the boundary condition

on the free surface (8) and transition conditions (9) on the liquid-solid interface, we get

$$w\int_{\Omega_F(t)}\frac{\partial \mathrm{T}_F}{\partial t}\psi_F\ dx+\int_{\Omega_F(t)}(\mathbf{u}\cdot\nabla)\mathrm{T}_F\ \psi_F\ dx + \frac{1}{\mathrm{Pe}_F}\int_{\Omega_F(t)}\nabla \mathrm{T}_F\cdot\nabla\psi_F\ dx+\int_{\Gamma_F(t)}\frac{\mathrm{Bi}}{\mathrm{Pe}_F}\ \mathrm{T}_F\ \psi_F\ d\gamma_F = -\frac{1}{\mathrm{Pe}_F}\frac{\lambda_S}{\lambda_F}\int_{\Gamma_S(t)}\frac{\partial \mathrm{T}_S}{\partial \nu_S}\psi_F\ d\gamma_F. \tag{17}$$

Similarly the weak form of the energy Eq. (7) is obtained by multiplying it with a test function $\psi_S \in H^1(\Omega_S(t))$. Then applying integration by parts, subsequently incorporating the transition conditions (9) on the liquid-solid interface and adiabatic condition (10) on $\Gamma_N(t)$, we get

$$\int_{\Omega_S(t)}\frac{\partial \mathrm{T}_S}{\partial t}\psi_S\ dx+\frac{1}{\mathrm{Pe}_S}\int_{\Omega_S(t)}\nabla \mathrm{T}_S\cdot\nabla\psi_S\ dx = \frac{1}{\mathrm{Pe}_S}\int_{\Gamma_S(t)}\frac{\partial \mathrm{T}_S}{\partial \nu_S}\ \psi_S\ d\gamma_S. \tag{18}$$

Further, by defining $\Omega(t) := \Omega_F(t)\cup\Omega_S\cup\Gamma_S(t)$ and

$$\mathbf{u}_T(x,t)=\begin{cases}\mathbf{u}(x,t) & \text{if} \quad x\in\Omega_F(t),\\ 0 & \text{if} \quad x\in\Omega_S,\end{cases}$$

$$\mathrm{T}(x,t)=\begin{cases}\mathrm{T}_F(x,t) & \text{if} \quad x\in\Omega_F(t),\\ \mathrm{T}_S(x,t) & \text{if} \quad x\in\Omega_S,\end{cases}$$

$$\mathrm{Pe}(x)=\begin{cases}\mathrm{Pe}_F & \text{if} \quad x\in\Omega_F(t),\\ \frac{\lambda_F}{\lambda_S}\mathrm{Pe}_F & \text{if} \quad x\in\Omega_S,\end{cases}$$

$$g(x)=\begin{cases}1 & \text{if} \quad x\in\Omega_F(t),\\ \frac{\lambda_S\mathrm{Pe}_S}{\lambda_F\mathrm{Pe}_F} & \text{if} \quad x\in\Omega_S.\end{cases}$$

$$\mathrm{T}_0(x)=\begin{cases}\mathrm{T}_{F,0}(x) & \text{if} \quad x\in\Omega_F(t),\\ \mathrm{T}_{S,0}(x) & \text{if} \quad x\in\Omega_S.\end{cases}$$

and rewriting the weak forms (17) and (18) into a one-field formulation, the weak form of the energy Eqs. (6) and (7) read:

For given $\Omega(0)$, $\mathbf{u}_T$ and T_0, find $\mathrm{T}\in H^1(\Omega(t))$ such that for all $\psi \in H^1(\Omega)$

$$\left(g\frac{\partial \mathrm{T}}{\partial t},\psi\right)_{\Omega(t)}+a_T(\mathbf{u}_T;\mathrm{T},\psi)+b_T(\mathrm{T},\psi)=0, \tag{19}$$

where

$$a_T(\mathbf{u}_T;\mathrm{T},\psi)=\int_{\Omega(t)}\frac{1}{\mathrm{Pe}}\ \nabla\mathrm{T}\cdot\nabla\psi\ dx+\int_{\Omega(t)}(\mathbf{u}\cdot\nabla)\mathrm{T}\ \psi\ dx,$$

$$b_T(\mathrm{T},\psi)=\mathrm{Bi}\int_{\Gamma_F(t)}\frac{1}{\mathrm{Pe}}\ \mathrm{T}\ \psi\ dx.$$

3.2. Finite element discretization

A brief description on the derivation of the discrete forms of (16) and (19) are presented here. Let $0=t^0<t^1<\cdots<t^N=\mathrm{I}$ be a decomposition of the given time interval [0, I] and $\delta t=t^{n+1}-t^n$, $n=0,\ldots,N-1$, be the uniform time step. The fractional-step-θ scheme, which is strongly A-stable and of second-order convergent on fixed domains (Turek, 1999), for the temporal discretization of the coupled system (16) and (19) is used. Applying the temporal discretization results in a sequence of stationary equations.

The finite element method is used for the spatial discretization. We assume that the sequence of spreading and recoiling of the impinging droplet is axisymmetric, and thus we first rewrite the volume and surface integrals in (16)–(19) into area and line integrals as described in Ganesan and Tobiska (2008). It allows to use two-dimensional finite elements for approximating the velocity, pressure and temperature in the cross-section of the domain. Further, it reduces the computational complexity in the mesh movement. The two-dimensional (cross-section) domain is triangulated using triangles, and the inf-sup stable Taylor-Hood finite element pair, that is, continuous piecewise quadratic polynomials and continuous piecewise linear polynomials for the discretization of the velocity components and pressure, respectively, is used. Further, the continuous piecewise quadratic polynomials is used for the discretization of temperature.

The ALE approach is used to track the free surface. Since the free surface is resolved by the computational mesh in the ALE approach, the spurious velocities if any can be suppressed when the surface force (curvature approximation) is incorporated into the scheme accurately (Ganesan et al., 2007). The application of the ALE approach adds additional mesh velocity convective term in the model equations, and the mesh velocity needs to be computed at every time step. Moreover, the mesh velocity is needed in every nonlinear iteration step, when an iteration of fixed point type is used to handle the nonlinear term in the Navier–Stokes equations. The mesh velocity is computed as the rate of change of the displacement of the mesh. The mesh displacement is obtained by first moving the boundary with the fluid velocity (kinematic condition), and then by solving the linear elasticity equation for the displacement of the inner mesh points as explained in Ganesan et al. (2014).

Maintaining a conforming mesh for $\Omega(t) := \Omega_F(t)\cup\Omega_S(t)$ during the mesh movement, especially along the liquid-solid interface is one of the challenging steps in the considered model. Due to the rolling motion of the droplet while spreading, the vertices on the free surface adjacent to the moving contact line will end up on the liquid-solid interface. This induces a non-conforming (non-matching) grid along the liquid-solid interface. An ad hoc algorithm proposed in Ganesan et al. (2014) is used to maintain a conforming mesh in the entire computation.

4. Numerical results

In this section a numerical investigation on the impingement and spreading of a 3D axisymmetric non-isothermal liquid droplet impact on a hot solid substrate with temperature-dependent contact angle is presented. Simulations and validations of isothermal liquid droplet impingement have been presented in Ganesan (2013); Ganesan and Tobiska (2008). Computations using sharp interface methods for non-isothermal droplet impingement have been presented and validated in Ganesan et al. (2014); 2015). Further, it has been assumed that the contact angle (incorporated in the weak form) is independent of the temperature. Nevertheless, as mentioned in the introduction, experiments in the literature show the temperature dependence on the contact angle (Adamson, 1973; Neumann, 1974; Petke and Ray, 1969; de Ruijter et al., 1998). Hence, in this paper, we assume that the contact angle is dependent on surface tension, which varies linearly with temperature. In due course of this section we would highlight the importance of this model for numerical simulations of non-isothermal liquid droplet impingement studies.

We first perform a mesh convergence study for a water droplet impinging on a hot solid substrate with $\theta_e^{ref}=120^\circ$. We then study the effects of temperature-dependent contact angle on the flow dynamics of droplet for different solid phase temperatures, Reynolds numbers, Weber numbers, Peclet numbers of solid phase and reference equilibrium contact angles. Further, the influence of these parameters on the total heat transfer from the solid substrate

Please cite this article as: J. Venkatesan et al., Effects of temperature-dependent contact angle on the flow dynamics of an impinging droplet on a hot solid substrate, International Journal of Heat and Fluid Flow (2016), http://dx.doi.org/10.1016/j.ijheatfluidflow.2016.10.003

to the liquid droplet is examined. The total heat

$$\int_0^t \int_{\Gamma_s(t)} \frac{1}{\mathrm{Pe}_S} \frac{\partial \mathrm{T}_S}{\partial \nu_S} \, d\gamma_S, \quad t \in (0, I]$$

is calculated using the variational form, and we refer to Ganesan et al. (2014) for the detailed derivation. We compare the results obtained with the contact angle models M1 (temperature-independent contact angle) and M2 (temperature-dependent contact angle) for each of the above cases. The difference in the numerical results obtained using M1 and M2 contact angle model determines the effect of temperature-dependent contact angle on the flow dynamics of the droplet. Unless specified, we use a constant time step $\delta t = 0.00025$, 200 vertices on the free surface with the initial edge size $h_0 = 0.000778929$. An arbitrary value $\mathcal{C}_1/\sigma_{ref} = 0.002$ is chosen. However, for experimental comparisons one has to choose an appropriate value. Further, we limit the maximum area of each cell in the mesh to 0.00625 during the triangulation (Shewchuk, 2002), and it results in 1364 and 2164 cells in the initial liquid and solid domains, respectively. This choice of initial mesh results in 5966 velocity, 810 pressure and 7443 temperature degrees of freedom. However, the number of cells and the number of degrees of freedom may vary during remeshing.

4.1. Mesh convergence

In this section, we perform a mesh convergence study for the proposed numerical scheme. We consider a hemispherical water droplet of diameter $d_0 = 3.34 \times 10^{-5}$ m on a hot solid substrate. We assume that the droplet is at rest initially. The contact angle is taken as $\theta_e^{ref} = 120^\circ$. The following material properties: $\rho = 1000$ kg/m^3, $\mu = 8.9 \times 10^{-4}$ Ns/m^2 and $\sigma_{ref} = 0.073$ N/m have been used. Also, we set $\mathrm{T}_{S,0} = 328$ K, $\mathrm{T}_{F,0} = 298$ K, $\mathrm{T}_\infty = 298$ K and $\mathrm{T}_{ref} = 323$ K. Using characteristic length $\mathrm{L} = d_0$, we get $\mathrm{Re} = 186$, $\mathrm{We} = 11.4$, $\mathrm{Fr} = 75387$, $\mathrm{Pe}_S = 200$, $\mathrm{Pe}_F = 40$ and $\mathrm{Bi} = 0.000116$. To perform a mesh convergence study, we vary the number of vertices on the free surface boundary. The initial mesh (L0) consists of 25 vertices on the free surface with $h_0 = 0.03141076$ and the successive mesh levels are generated by doubling the vertices on the free surface and halving the mesh size of the previous level mesh. Five variants with different number of vertices on the free surface are used: (i) L0 with 25 vertices (ii) L1 with 50 vertices, (iii) L2 with 100 vertices, (iv) L3 with 200 vertices and (v) L4 with 400 vertices. Mesh dependent slip number, $\beta_\epsilon = 1.46/2h_0$ is used in these computations, which is obtained from the following slip relation (Venkatesan and Ganesan, 2015)

$$\beta_\epsilon = \frac{\beta}{2h_0}, \qquad \beta = \alpha \mathrm{Re}^\gamma + \lambda \mathrm{We}^\delta, \tag{20}$$

where

$$\alpha = 4.796842276577 \times 10^5, \qquad \gamma = -3.339370111853,$$
$$\lambda = 2.021796892969 \times 10^1, \qquad \delta = -1.142224345078.$$

The slip number (β_ϵ) depends on the Reynolds number (Re), Weber number (We) and the initial mesh size (h_0). The wetting diameter, dynamic contact angle and the total heat flow curves for all the mesh levels are shown in Fig. 2.

Since the initial contact angle of the droplet is 90°, the contact angle and wetting diameter are not in equilibrium. Hence over a period of time, the droplet slowly oscillates and attains its equilibrium state which can be seen in Fig. 2(a). We can clearly observe the mesh convergence with L3 and L4 meshes. From the dynamic contact angle curves in Fig. 2(b), we observe that the equilibrium contact angles of L3 and L4 meshes are tending towards 120°, which is the same value that we have imposed in the weak formulation. From the total heat curves Fig. 2(c), we observe that a mesh independent solution can be obtained even with L0 mesh.

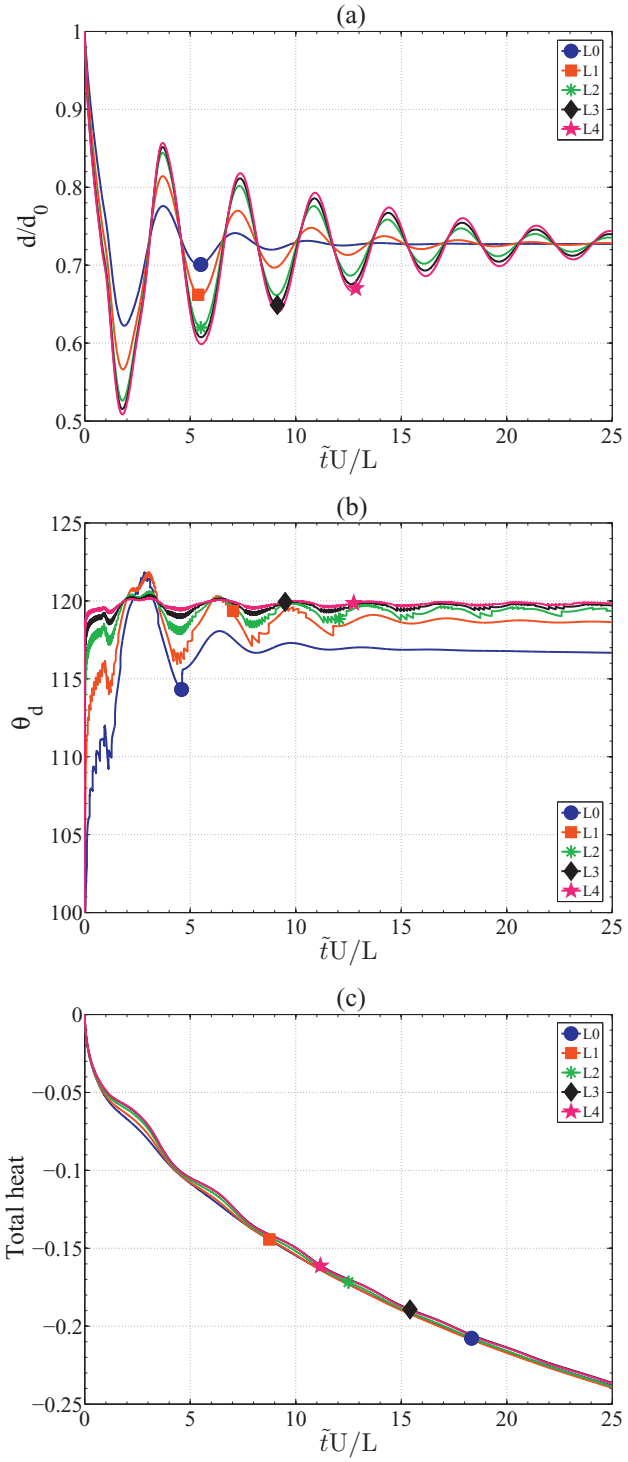

Fig. 2. Computationally obtained wetting diameter (a), dynamic contact angle (b) and total heat (c) for $\mathrm{Re} = 186$, $\mathrm{We} = 11.4$, $\mathrm{Fr} = 75387$, $\mathrm{Bi} = 0.000116$, $\mathrm{Pe}_F = 40$, $\mathrm{Pe}_S = 200$ and $\theta_e^{ref} = 120^\circ$ with different number of points on the free surface boundary.

However, since our aim is also to accurately capture the flow dynamics of a non-isothermal impinging droplet, we use L3 mesh (200 vertices) in all computations.

4.2. Effect of the temperature-dependent contact angle

In this section, we study the effects of temperature-dependent contact angle on the flow dynamics of a non–isothermal impinging

Table 1
Percentage maximum relative difference in the dimensionless wetting diameter and total heat between the two models for various equilibrium contact angles.

θ_e^{ref}	δ_{wd}(%)	δ_{th}(%)
15	3.71	2.75
67	2.03	1.71
90	0.84	0.14
105	3.42	0.65
120	9.08	6.02

droplet for different equilibrium contact angles $\left(\theta_e^{ref}\right)$. The aim of this study is to identity the equilibrium contact angle for which the effect of temperature-dependent contact angle is maximum. We consider a spherical liquid droplet of diameter $d_0 = 3.34 \times 10^{-5}$ m impinging on a hot solid substrate with an impact speed $u_{imp} = 4.97$ m/s. We use the following material properties: $\rho = 1000$ kg/m^3, $\mu = 8.9 \times 10^{-4}$ Ns/m^2 and $\sigma_{ref} = 0.073$ N/m. Also, we set $\beta = 3.116/2h_0$, $T_{S,0} = 328$ K, $T_{F,0} = 298$ K, $T_\infty = 298$ K and $T_{ref} = 323$ K. Using characteristic velocity $U = u_{imp}$ and characteristic length $L = d_0$, we get Re = 186, We = 11.4, Fr = 75387, $Pe_S = 200$, $Pe_F = 40$ and Bi = 0.000116. We consider the following five variants for the equilibrium contact angle: (i) $\theta_e^{ref} = 15°$, (ii) $\theta_e^{ref} = 67°$, (iii) $\theta_e^{ref} = 90°$, (iv) $\theta_e^{ref} = 105°$ and (v) $\theta_e^{ref} = 120°$. Fig. 3 shows the wetting diameter (a), dynamic contact angle (b) and total heat (c) transfer from the solid substrate into the liquid droplet. Note that the results obtained using both the temperature independent contact angle (M1) and the temperature dependent contact angle (M2) models are shown in Fig. 3.

From Fig. 3(a), we can observe that the maximum and equilibrium wetting diameter decreases with increase in the equilibrium contact angle. Also, the recoiling effect is observed only with partially wetting and non–wetting liquids. Recoiling effect increases with increase in the equilibrium contact angle. For the variant $\theta_e^{ref} = 90°$, there is no variation in the wetting diameter between M1 and M2 contact angle models. This is because, when $\theta_e^{ref} = 90°$, temperature has no effect on the dynamic contact angle as discussed in Section 2.3. For the variants $\theta_e^{ref} = 15°$ and $\theta_e^{ref} = 67°$, we can observe that the maximum wetting diameter obtained with M2 model is less than that with M1 model. This is consistent with our prediction that for wetting and partially wetting liquids ($\theta_e^{ref} < 90°$) and when $\tilde{T}_F$ is less than reference temperature, the dynamic contact angle for M2 model is greater than M1 model. We also predicted that the difference between the maximum wetting diameters with M1 and M2 contact angles be more visible for highly wetting liquids, and it can be observed in the variant $\theta_e^{ref} = 15°$ when compared to the variant $\theta_e^{ref} = 67°$. For the variants $\theta_e^{ref} = 105°$ and $\theta_e^{ref} = 120°$, we can observe that the wetting diameter during recoiling phase obtained with M2 model is greater than obtained with M1 model. This is also consistent with our prediction that for non–wetting liquids ($\theta_e^{ref} > 90$) and when $\tilde{T}_F$ is less than the reference temperature, the dynamic contact angle for M1 model is greater than M2 model. We also predicted the difference to be more visible for highly non–wetting liquids and it can be observed for the case $\theta_e^{ref} = 120°$. Note that we have considered the equilibrium contact angles till 120° only, as any value above that leads to splitting of the droplet during spreading and recoiling for the given Reynolds and Weber numbers. In order to perform a quantitative assessment on the effect of temperature-dependent contact angle, Table 1 shows the maximum relative difference in the wetting diameter and total heat between the two

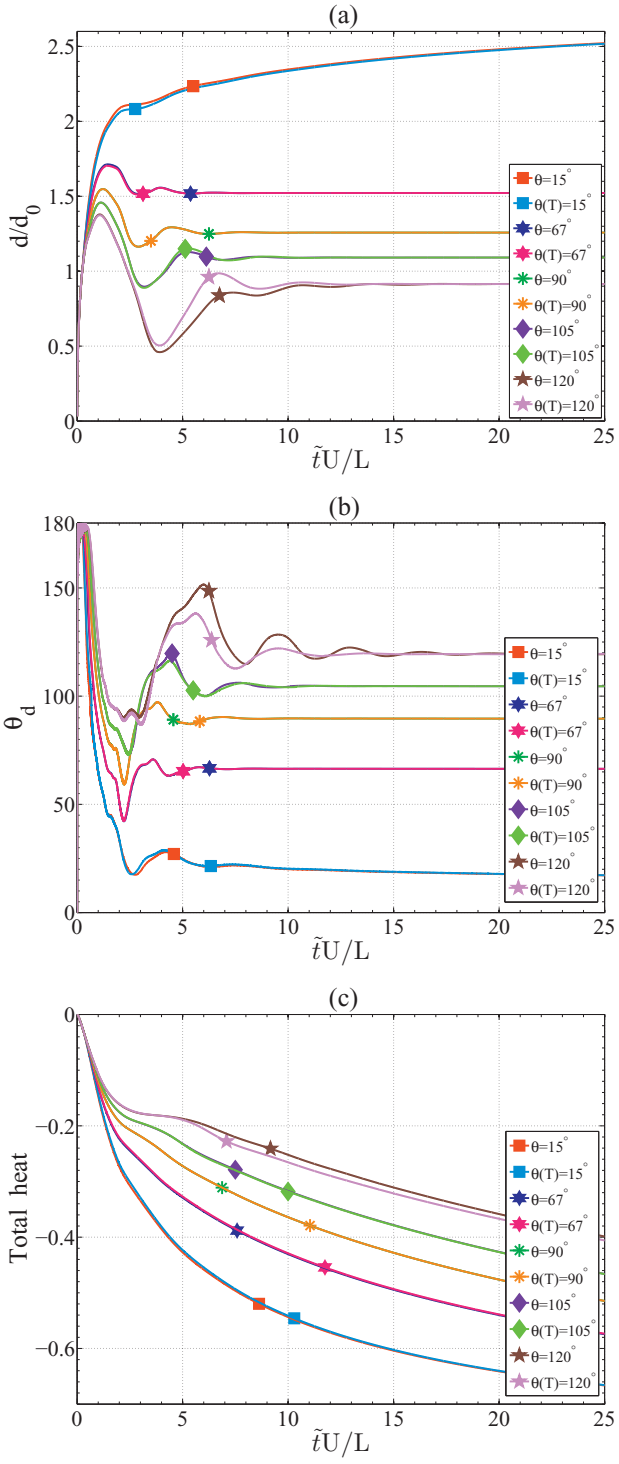

Fig. 3. Computationally obtained wetting diameter (a), dynamic contact angle (b) and total heat (c) with Re = 186, We = 11.4, Fr = 75387, Bi = 0.000116, $Pe_F = 40$, $Pe_S = 200$ and different equilibrium contact angles $\theta_e^{ref} = 15°$, $\theta_e^{ref} = 67°$, $\theta_e^{ref} = 90°$, $\theta_e^{ref} = 105°$ and $\theta_e^{ref} = 120°$ for both M1 and M2 contact angle models.

contact angle models that are calculated as follows

$$\delta_{wd} = \max_{t\in[0,l]} \left| \frac{d^{M2}(t) - d^{M1}(t)}{d^{M1}(t)} \right| \times 100\,\%,$$

$$\delta_{th} = \max_{t\in[0,l]} \left| \frac{th^{M2}(t) - th^{M1}(t)}{th^{M1}(t)} \right| \times 100\%.$$

Please cite this article as: J. Venkatesan et al., Effects of temperature-dependent contact angle on the flow dynamics of an impinging droplet on a hot solid substrate, International Journal of Heat and Fluid Flow (2016), http://dx.doi.org/10.1016/j.ijheatfluidflow.2016.10.003

Here, the superscripts M1 and M2 on the wetting diameter d (also on the total heat) denote that the values are obtained with the contact angle models M1 and M2, respectively. The maximum difference in the wetting diameter is 9.08% for the variant $\theta_e^{ref} = 120^\circ$, which is quite significant. On comparing the results between M1 and M2 contact angle models for the considered equilibrium contact angles, we can observe that the effect of temperature-dependent contact angle is more visible in non–wetting and highly wetting liquids.

An interesting observation is that the effect of temperature-dependent contact angle is visible only during the recoiling stage and almost negligible in the initial spreading stage. During the initial spreading stage, the droplet motion is dominated by the inertia of the impingement and the surface force is less dominant. However, the surface tension opposes the spreading and the droplet recoils back when the surface force dominates. Since the contact angle is dependent on the temperature-dependent surface tension, the effect of temperature-dependent contact angle can be observed only when the surface force dominates, i.e. during the recoiling phase and this is exactly what we observe in Fig. 3(a).

Next, from Fig. 3(b), we can observe that the temperature-dependent contact angle effects on the dynamic contact angle are more visible for the variant $\theta_e^{ref} = 120^\circ$, i.e. for non–wetting liquids. A similar variation is observed between the two contact angle models as observed in the wetting diameter curve. Further, from Fig. 3(c) and Table 1, we can observe that the effects of temperature-dependent contact angle on the total heat transfer from the solid substrate into the liquid droplet is maximum for the variant $\theta_e^{ref} = 120^\circ$, which is about 6.02%. We can also observe that the total heat decreases with an increase in the equilibrium contact angle. Since the maximum as well as the equilibrium wetting diameter decrease with an increase in θ_e^{ref}, the liquid-solid interface area over which the heat transfer occurs is reduced.

Based on the above observations, we can conclude that the effect of temperature-dependent contact angle is higher for non–wetting and highly wetting liquid. However, comparatively non-wetting liquids ($\theta_e^{ref} > 90^\circ$) show significant thermal effects due to M2 contact angle model. Also, it is more sensitive during the recoiling phase and not during initial spreading phase as the effect of temperature-dependent contact angle is more when the surface force dominates the inertial force in the droplet. Precisely, the maximum effect of the temperature-dependent contact angle on the wetting diameter is about 9.08% and on the total heat transfer is 6.02% for the considered flow parameters. Note that we have used $\mathcal{C}_1/\sigma_{ref} = 0.002$, where $\mathcal{C}_1$ is the negative rate of change of surface tension with temperature in the computations. The effect of temperature-dependent contact angle is directly dependent on the temperature-dependent surface tension. Hence, a greater effect of the temperature–dependence of contact angle could be observed if we choose a higher value of $\mathcal{C}_1/\sigma_{ref}$. As $\theta_e^{ref} = 120^\circ$ variant shows the maximum thermal effects due to M2 contact angle model from the considered equilibrium contact angles, we consider this as the model case in the subsequent sections and study the effects of temperature-dependent contact angle for different solid phase temperatures, Reynolds numbers, Weber numbers and solid phase Peclet numbers.

We now present the contours of the pressure, velocity and the temperature distribution for the variant $\theta_e^{ref} = 120^\circ$. Fig. 4 depicts the pressure contours in the droplet at different instances (dimensionless time) t = 0.1, 1, 4, 6, 15. Initially the pressure variation is large near the contact line. However, the distribution of the pressure becomes almost uniform when the droplet reaches its equilibrium state. Both M1 and M2 contact angle models have almost identical pressure distribution at time instances t = 0.1 and 1.0, i.e. when the droplet is in the initial spreading stage dominated by the inertial forces. However, at time instances t = 4.0 and 6.0, we can observe differences in the pressure distribution. Also note that, the maximum value of pressure in the droplet is higher in the M2 model. Next, the contour lines of the magnitude of the velocity are depicted in Fig. 5. By comparing the contour lines of M1 and M2 models, we can observe that there is a significant variation in the velocity distribution at t = 4.0, 6.0 and 15.0. Further, the temperature distribution in the droplet is depicted in Fig. 6. Both M1 and M2 contact angle models have very slight difference in the temperature distribution at all the considered time instances. Note the minimum values of temperature at each instant is higher for the M2 model, which indicates that the overall temperature in the droplet is higher for M2 contact angle model.

4.3. Effect of solid phase initial temperature

In this section, we study the effect of temperature-dependent contact angle on the flow dynamics of droplet for different solid phase initial temperatures. We consider a liquid droplet of diameter $d_0 = 3.34 \times 10^{-5}$ m impinging on a hot solid substrate with an impact speed $u_{imp} = 4.97$ m/s. We use the following material properties: $\rho = 1000$ kg/m^3, $\mu = 8.9 \times 10^{-4}$ Ns/m^2 and $\sigma_{ref} = 0.073$ N/m. Also, we set $\beta = 3.116/2h_0$, $T_{F,0} = 298$ K, $T_\infty = 298$ K and $T_{ref} = 323$ K. Using characteristic velocity $U = u_{imp}$ and characteristic length $L = d_0$, we get Re = 186, We = 11.4, Fr = 75387, $Pe_S = 200$, $Pe_F = 40$ and Bi = 0.000116. We consider the following four variants for solid phase temperature : (i) $T_{S,0} = 328$ K, (ii) $T_{S,0} = 338$ K, (iii) $T_{S,0} = 348$ K and (iv) $T_{S,0} = 358$ K. Further, we consider two variants for the contact angle, $\theta_e^{ref} = 15^\circ$ and $\theta_e^{ref} = 120^\circ$. Figs. 7 and 8 shows the wetting diameter (a), magnified view of wetting diameter at the equilibrium or during the recoiling phase (b) and the total heat (c) transfer from the solid substrate into the liquid droplet for contact angles $\theta_e^{ref} = 15^\circ$ and $\theta_e^{ref} = 120^\circ$ respectively.

From Fig. 7(a), we can observe that the effect of the solid phase temperature is negligible on the flow dynamics of the droplet for the variant $\theta_e^{ref} = 15^\circ$. However, from the magnified view of the wetting diameter of droplet as it approaches equilibrium, we can observe that the wetting diameter increases with increase in the solid phase temperature and decreases for the temperature-dependent contact angle. From the total heat curve, we can clearly observe that more heat is transferred from the solid into liquid phase at higher solid phase temperatures. Moreover, there doesn't seem to be any visible effect of temperature-dependent contact angle on the total heat transfer for different solid phase temperatures with $\theta_e^{ref} = 15^\circ$. For the variant $\theta_e^{ref} = 120^\circ$, the temperature-dependent contact angle significantly influences the flow dynamics in the recoiling phase as observed in the previous section. But the equilibrium wetting diameter remains unaffected by the solid phase temperature changes and temperature-dependent contact angle. However, the effect of temperature-dependent contact angle on the flow dynamics is similar for the considered solid phase temperatures. Hence, in the subsequent sections we perform all the computations with $T_{S,0} = 328$ K. A close up view of the wetting diameter when the droplet is in the recoiling stage, reveals that the temperature-dependent contact angle leads to higher wetting diameter for the variant $\theta_e^{ref} = 120^\circ$. The total heat transfer from the solid into the liquid phase increases with an increase in the solid phase temperature, as observed in Fig. 8(c).

4.4. Effect of Reynolds number

In this section, we study the effects of temperature-dependent contact angle on the flow dynamics of droplet for different Reynolds numbers. By varying the Reynolds number, we vary only the viscosity and keep all other parameters constant. We consider

Please cite this article as: J. Venkatesan et al., Effects of temperature-dependent contact angle on the flow dynamics of an impinging droplet on a hot solid substrate, International Journal of Heat and Fluid Flow (2016), http://dx.doi.org/10.1016/j.ijheatfluidflow.2016.10.003

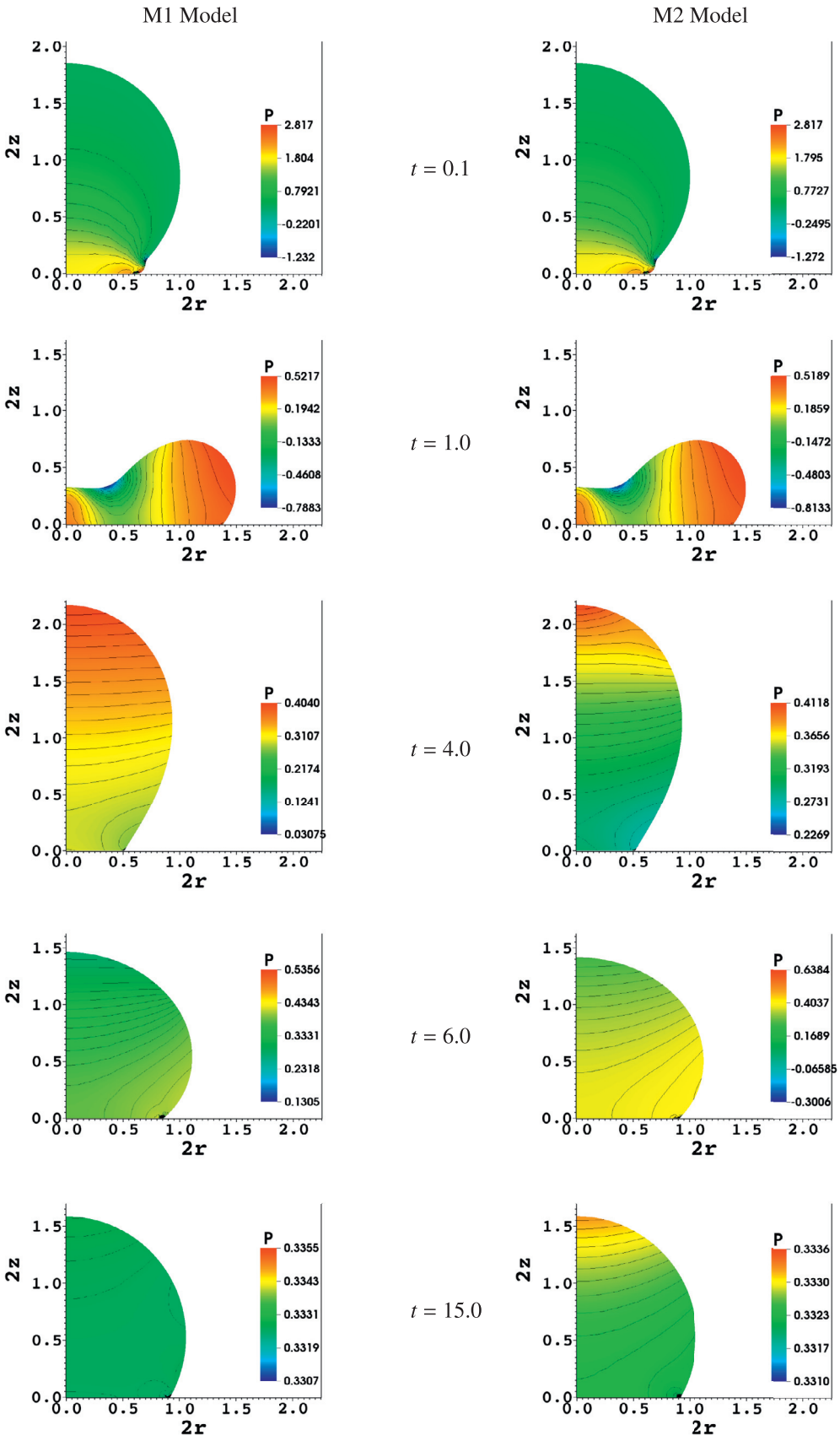

Fig. 4. Pressure contours in the impinging droplet with $\theta_e^{ref} = 120^\circ$ at dimensionless time t = 0.1, 1, 4, 6, 15 from the top for M1 and M2 contact angle models.

Please cite this article as: J. Venkatesan et al., Effects of temperature-dependent contact angle on the flow dynamics of an impinging droplet on a hot solid substrate, International Journal of Heat and Fluid Flow (2016), http://dx.doi.org/10.1016/j.ijheatfluidflow.2016.10.003

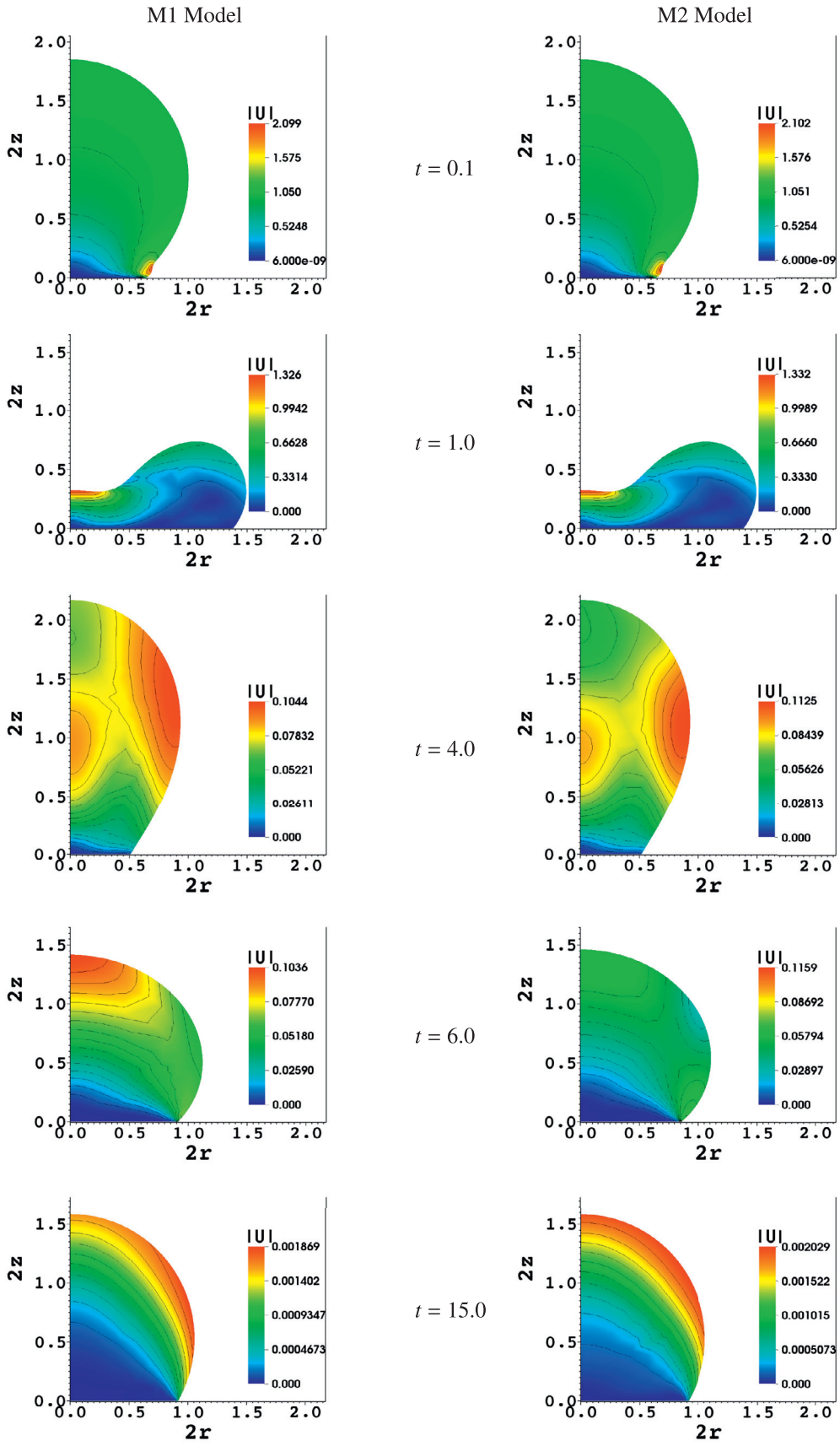

Fig. 5. Velocity (magnitude) contours in the impinging droplet with $\theta_e^{ref} = 120^\circ$ at dimensionless time t = 0.1, 1, 4, 6, 15 from the top for M1 and M2 contact angle models.

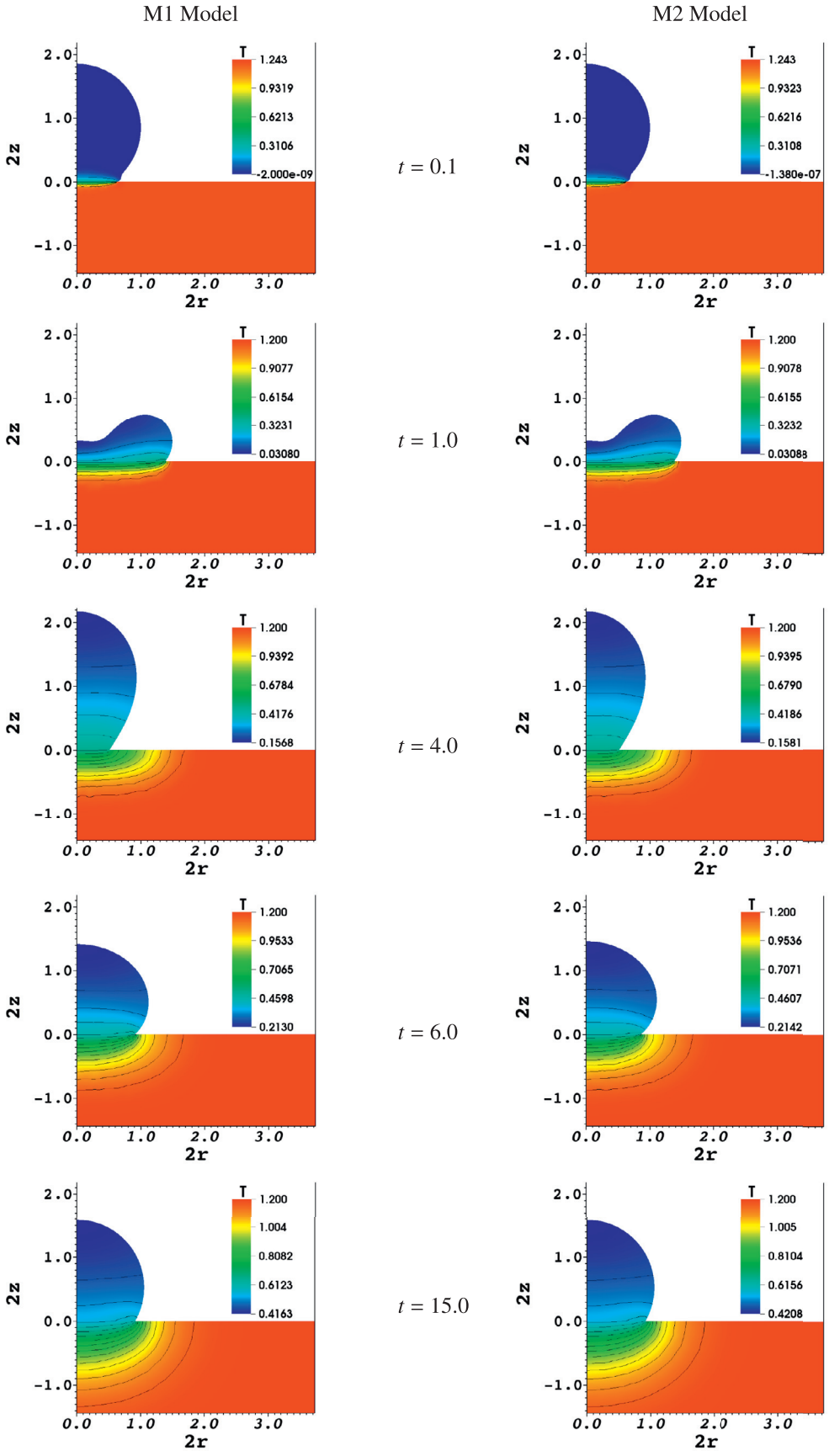

Fig. 6. Temperature contours in the impinging droplet with $\theta_e^{ref} = 120^\circ$ at dimensionless time t = 0.1, 1, 4, 6, 15 from the top for M1 and M2 contact angle models.

Please cite this article as: J. Venkatesan et al., Effects of temperature-dependent contact angle on the flow dynamics of an impinging droplet on a hot solid substrate, International Journal of Heat and Fluid Flow (2016), http://dx.doi.org/10.1016/j.ijheatfluidflow.2016.10.003

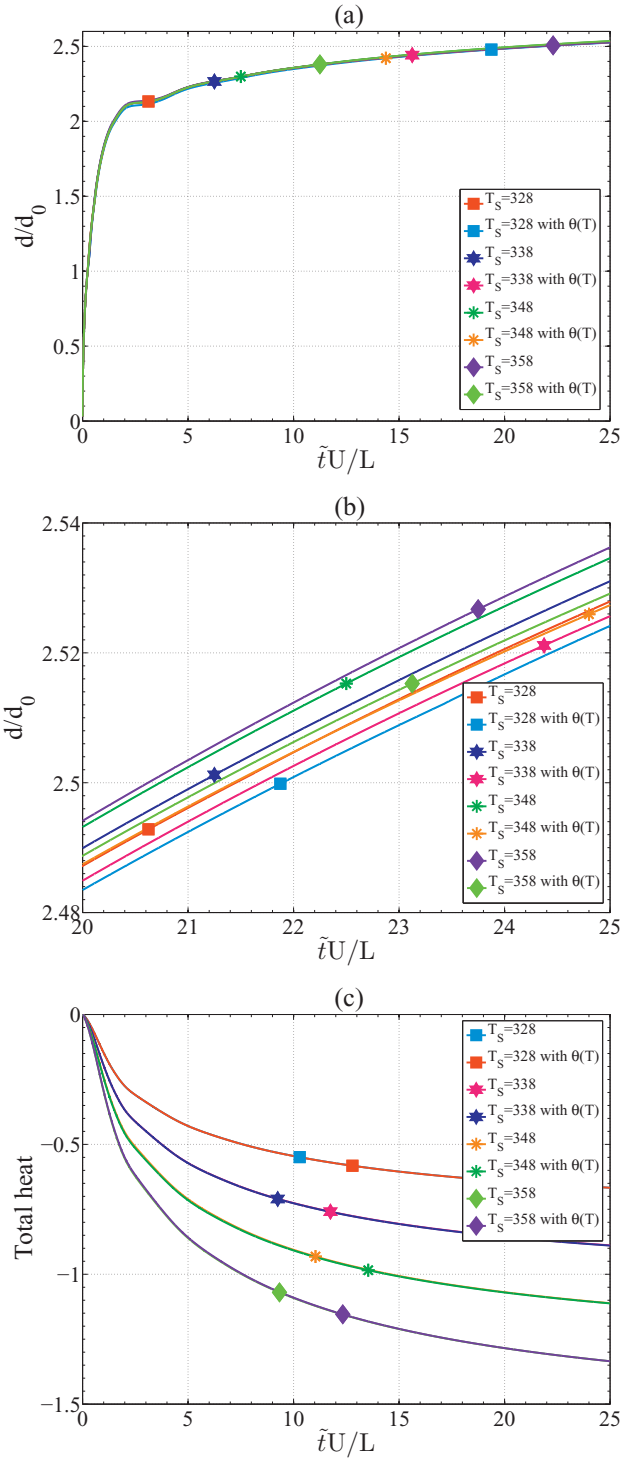

Fig. 7. Computationally obtained wetting diameter (a), magnified view of wetting diameter at the equilibrium (b) and total heat (c) with Re = 186, We = 11.4, Fr = 75387, Bi = 0.000116, $Pe_F = 40$, $Pe_S = 200$, $\theta_e^{ref} = 15^\circ$ and different solid phase temperatures $T_{S,0} = 328$ K, $T_{S,0} = 338$ K, $T_{S,0} = 348$ K and $T_{S,0} = 358$ K for both M1 and M2 contact angle models.

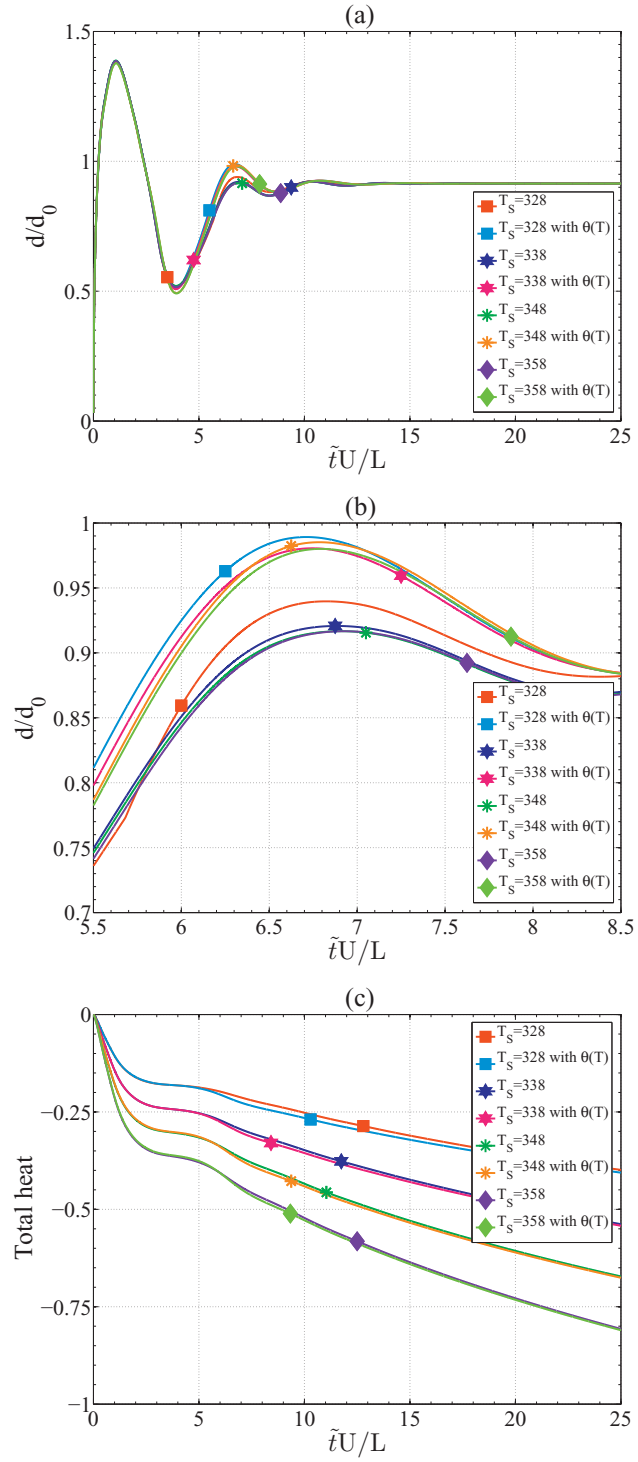

Fig. 8. Computationally obtained wetting diameter (a), magnified view of wetting diameter during the recoiling phase (b) and total heat (c) with Re = 186, We = 11.4, Fr = 75387, Bi = 0.000116, $Pe_F = 40$, $Pe_S = 200$, $\theta_e^{ref} = 120^\circ$ and different solid phase temperatures $T_{S,0} = 328$ K, $T_{S,0} = 338$ K, $T_{S,0} = 348$ K and $T_{S,0} = 358$ K for both M1 and M2 contact angle models.

a liquid droplet of diameter $d_0 = 3.34 \times 10^{-5}$ m impinging on a hot solid substrate with an impact speed $u_{imp} = 4.97$ m/s. Further, the equilibrium contact angle is taken as $\theta_e^{ref} = 120^\circ$. We use the following material properties: $\rho = 1000$ kg/m^3 and $\sigma_{ref} = 0.073$ N/m. Also, we set $T_{S,0} = 328$ K, $T_{F,0} = 298$ K, $T_\infty = 298$ K and $T_{ref} = 323$ K. Using characteristic velocity $U = u_{imp}$ and characteristic length $L = d_0$, we get We = 11.4, Fr = 75387, $Pe_S = 200$, $Pe_F = 40$ and Bi = 0.000116.

We consider the following four variants for the Reynolds number: (i) Re = 50, (ii) Re = 100 and (iii) Re = 186. The slip number used in the computations is based on the mesh-dependent slip relation (Venkatesan and Ganesan, 2015). The numerical results obtained for different Reynolds numbers for both M1 and M2 con-

Please cite this article as: J. Venkatesan et al., Effects of temperature-dependent contact angle on the flow dynamics of an impinging droplet on a hot solid substrate, International Journal of Heat and Fluid Flow (2016), http://dx.doi.org/10.1016/j.ijheatfluidflow.2016.10.003

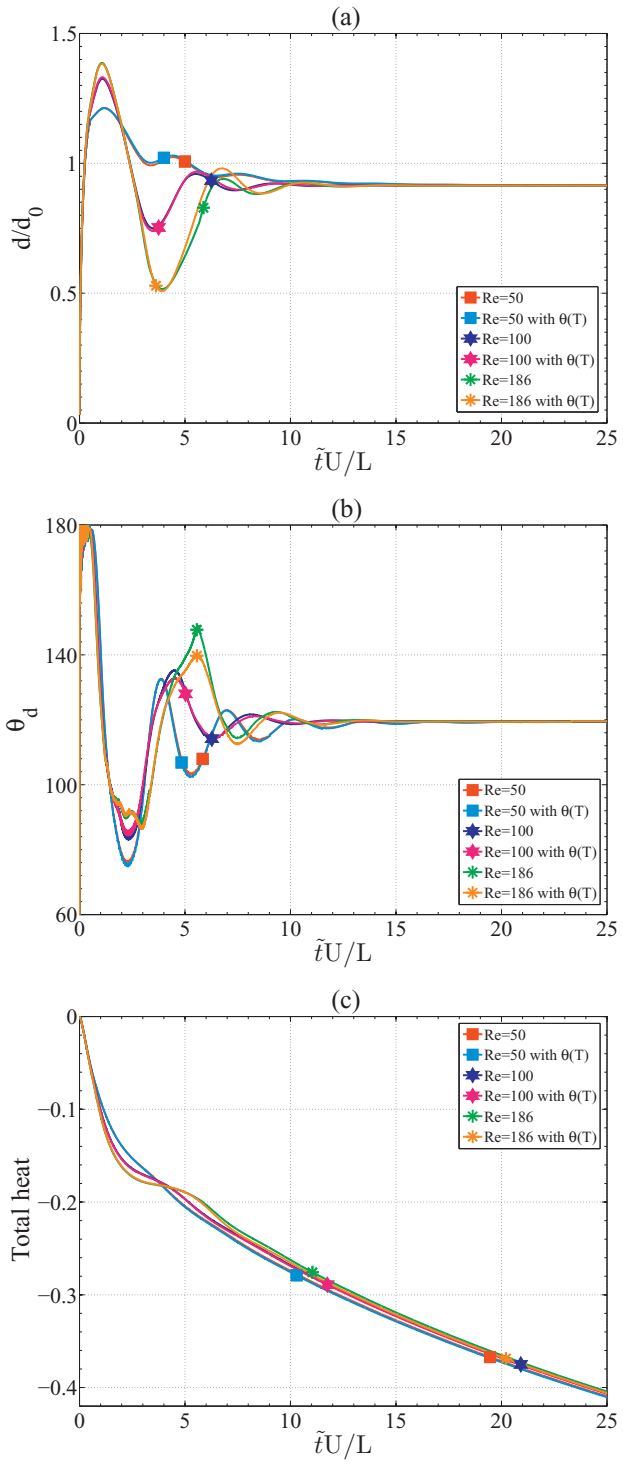

Fig. 9. Computationally obtained wetting diameter (a), dynamic contact angle (b) and total heat (c) with $\theta_e^{ref} = 120^\circ$, We = 11.4, Fr = 75387, Bi = 0.000116, $Pe_F = 40$, $Pe_S = 200$ and different Reynolds numbers Re = 50, Re = 100 and Re = 186 for both M1 and M2 contact angle models.

tact angle models are shown in Fig. 9. Note that we have considered the Reynolds number till 186 only, as any value above leads to splitting of the droplet.

From Fig. 9(a), we can observe that the maximum wetting diameter increases with an increase in the Reynolds number. Since the kinetic energy of the droplet increases, the wetting diameter is more with an increase in the Reynolds number. However, the equilibrium wetting diameter remains the same. Also, recoiling effect increases with an increase in the Reynolds number. By comparing the wetting diameter curves for the two contact angle models M1 and M2, we can observe that the effect of temperature-dependent contact angle increases with an increase in the Reynolds number. The same can be quantitatively observed in Table 2, which provides the percentage maximum difference in the wetting diameter and the total heat for the two contact angle models.

Table 2
Percentage maximum relative difference in the dimensionless wetting diameter and total heat between the two models for various Reynolds numbers.

Re	δ_{wd}(%)	δ_{th}(%)
50	2.38	0.57
100	3.05	0.71
186	9.08	6.02

From Fig. 9(b), we can observe that the dynamic contact angle oscillates about its equilibrium value during the spreading and recoiling phase. Also the oscillations increase with an increase in the Reynolds number which is due to a greater kinetic energy. The effects of temperature-dependent contact angle observed are similar to as observed in the wetting diameter curves. From Fig. 9(c), we can observe that the total heat transfer from the solid substrate into the liquid phase decreases slightly with an increase in the Reynolds number. Since the droplet reaches to maximum wetting diameter quickly and recoils rapidly when the Reynolds number is increased, the liquid-solid interface area over which the heat transferred reduces. Thus, the total heat transfer becomes less when the Reynolds number is increased. In short, we can observe and conclude that an increase in the Reynolds number results in a greater effect of temperature-dependent contact angle on the flow dynamics of the droplet.

4.5. Effect of Weber number

In this section, we study the effect of temperature-dependent contact angle on the flow dynamics of droplet for different Weber numbers, that is by varying the reference surface tension and keeping other parameters as constant. We consider a liquid droplet of diameter $d_0 = 3.34 \times 10^{-5}$ m impinging on a hot solid substrate with an impact speed $u_{imp} = 4.97$ m/s. Further, the contact angle is taken as $\theta_e^{ref} = 120^\circ$. We use the following material properties: $\rho = 1000\,kg/m^3$ and $\mu = 8.9 \times 10^{-4}\,Ns/m^2$. Also, we use $T_{S,0} = 328$ K, $T_{F,0} = 298$ K, $T_\infty = 298$ K and $T_{ref} = 323$ K. Using characteristic velocity $U = u_{imp}$ and characteristic length $L = d_0$, we get Re = 186, Fr = 75387, $Pe_S = 200$, $Pe_F = 40$ and Bi = 0.000116. The slip value used in computations is based on the mesh-dependent slip relation (Venkatesan and Ganesan, 2015). We consider the following five variants for the Weber number: (i) We = 2.0, (ii) We = 5.0, (iii) We = 11.4, (iv) We = 20.0 and (v) We = 50.0. The numerical results obtained for different Weber numbers for both M1 and M2 contact angle models are shown in Fig. 10.

From Fig. 10(a), we can observe that the maximum wetting diameter increases with an increase in the Weber number. Since the capillary force of the droplet decreases with an increase in the Weber number, it leads to a larger spreading and hence greater wetting diameter. Also, recoiling effect increases with an increase in the Weber number. By comparing the wetting diameter curves of the two contact angle models M1 and M2, we can observe that the effects due to the temperature-dependent contact angle increases with an increase in the Weber number initially, say till We = 11.4 and then decreases with an increase in the Weber number. The same can also be observed from Table 3. Also we observe that the

Please cite this article as: J. Venkatesan et al., Effects of temperature-dependent contact angle on the flow dynamics of an impinging droplet on a hot solid substrate, International Journal of Heat and Fluid Flow (2016), http://dx.doi.org/10.1016/j.ijheatfluidflow.2016.10.003

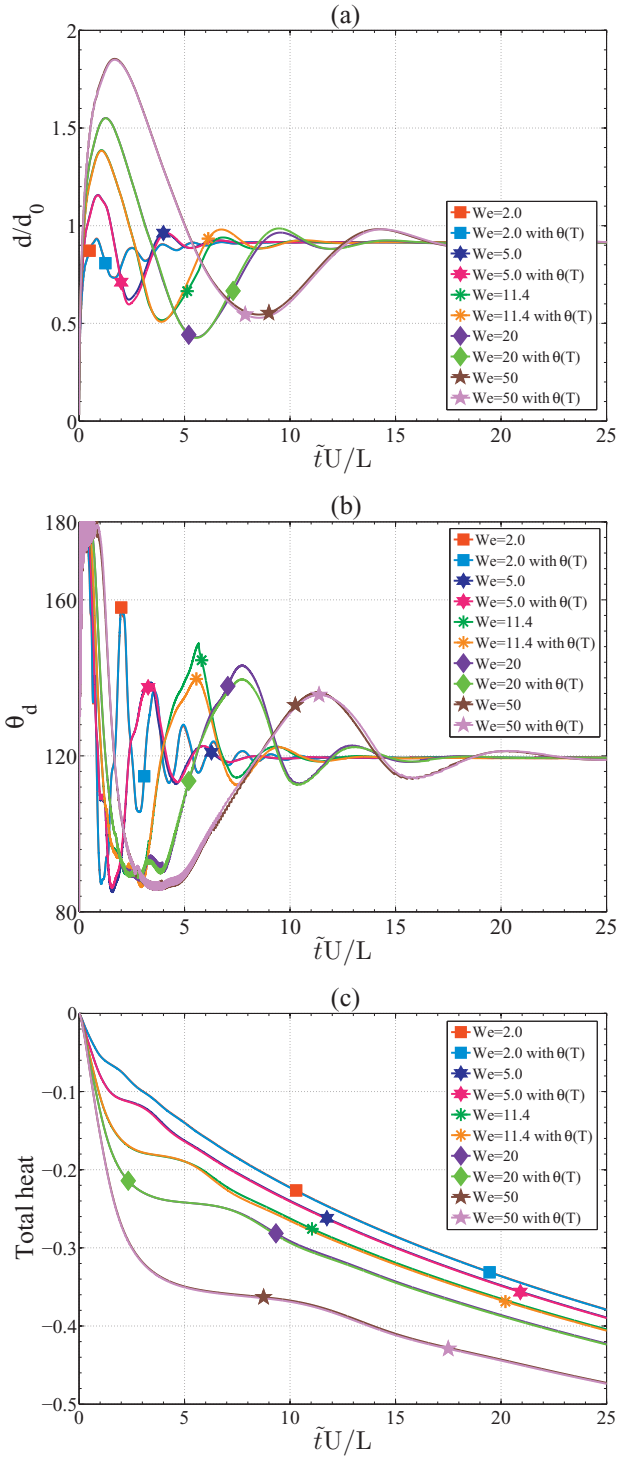

Fig. 10. Computationally obtained wetting diameter (a), dynamic contact angle (b) and total heat (c) with $\theta_e^{ref} = 120^\circ$, Re = 186, Fr = 75387, Bi = 0.000116, $Pe_F = 40$, $Pe_S = 200$ and different Weber numbers We = 2.0, We = 5.0, We = 11.4, We = 20.0 and We = 50.0 for both M1 and M2 contact angle models.

effects of the temperature-dependent contact angle are more visible in the recoiling phase and almost negligible in the spreading phase as observed in the previous sections.

From Fig. 10(b), we can observe that the dynamic contact angle oscillates about its equilibrium value during the spreading and recoiling phase. Also the oscillations increase with an increase in the Weber number. The effects of the temperature-dependent contact angle are similar as observed in the wetting diameter curves. From Fig. 10(c), we can observe that the total heat transfer from the solid substrate into the liquid phase increases with an increase in the Weber number. This depends on the maximum wetting diameter which increases with an increase in the Weber number, and thus increasing the liquid-solid interface area over which the heat transfer occurs. However, the increase is quite high compared to the variants used for the Reynolds number.

Table 3
Percentage maximum difference in the dimensionless wetting diameter and total heat between the two models for various Weber numbers .

We	δ_{wd}(%)	δ_{th}(%)
2	3.8	0.51
5	4.48	1.44
11.4	9.08	6.02
20	3.9	0.8
50	3.12	0.56

Table 4
Percentage maximum difference in the dimensionless wetting diameter and total heat between the two models for various solid phase Peclet numbers.

Pe_S	δ_{wd}(%)	δ_{th}(%)
100	10.79	7.36
200	9.08	6.02
400	4.33	1.47

4.6. Effect of solid phase Peclet number

In this section, we study the effect of temperature-dependent contact angle on the flow dynamics of droplet for different solid phase Peclet numbers, in particular by varying the conductivity of solid phase and keeping the other parameters as constant. We consider a liquid droplet of diameter $d_0 = 3.34 \times 10^{-5}$ m impinging on a hot solid substrate with an impact speed $u_{imp} = 4.97$ m/s. Further, the equilibrium contact angle is taken as $\theta_e^{ref} = 120^\circ$. We use the following material properties: $\rho = 1000$ kg/m^3, $\mu = 8.9 \times 10^{-4}$ Ns/m^2 and $\sigma_{ref} = 0.073$ N/m. We also use $T_{S,0} = 328$ K, $T_{F,0} = 298$ K, $T_\infty = 298$ K and $T_{ref} = 323$ K. Using characteristic velocity $U = u_{imp}$ and characteristic length $L = d_0$, we get Re = 186, We=11.4, Fr = 75387, Bi = 0.000116 and $Pe_F = 40$. We consider the following three variants for the solid phase Peclet number: (i) $Pe_S = 100$, (ii) $Pe_S = 200$ and (iii) $Pe_S = 400$. The numerical results obtained with the three variants of solid phase Peclet numbers for both M1 and M2 contact angle models are shown in Fig. 11.

From Fig. 11(a), we can observe that the maximum and equilibrium wetting diameter remains the same irrespective of the solid phase Peclet number used. However, during the recoiling stage the Peclet number has visible effect on the wetting diameter. Comparing the wetting diameter curves of the two contact angle models M1 and M2, we can observe that the effects due to the temperature-dependent contact angle remains similar in the considered Peclet numbers. However, the magnitude of the effect varies and it decreases with an increase in the Peclet number as observed in Table 4.

From Fig. 11(b), we can observe that the dynamic contact angle oscillates about its equilibrium value during the spreading and recoiling phase. Also the oscillations do not increase significantly with an increase in the Peclet number, unlike in the variants of Reynolds and Weber numbers. The effects of temperature-dependent contact angle are similar to as observed in the wetting diameter curves. From Fig. 11(c), we can observe that the to-

Please cite this article as: J. Venkatesan et al., Effects of temperature-dependent contact angle on the flow dynamics of an impinging droplet on a hot solid substrate, International Journal of Heat and Fluid Flow (2016), http://dx.doi.org/10.1016/j.ijheatfluidflow.2016.10.003

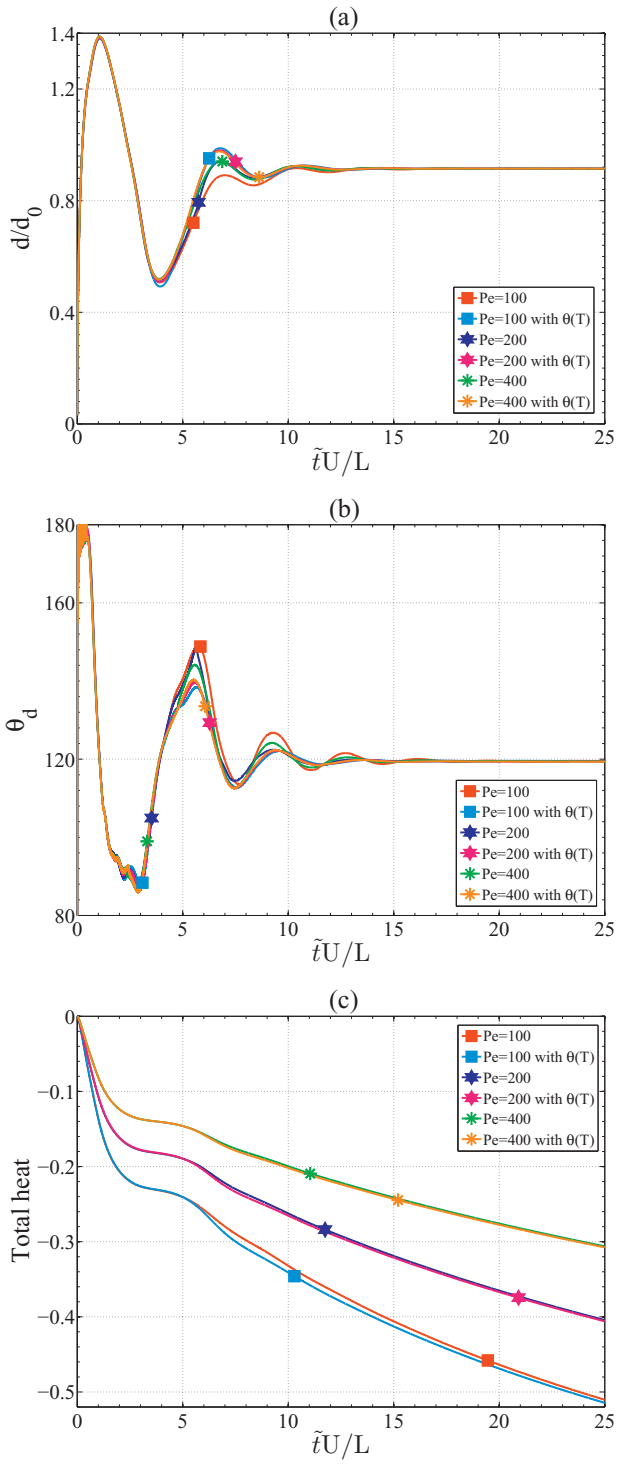

Fig. 11. Computationally obtained wetting diameter (a), dynamic contact angle (b) and total heat (c) with $\theta_e^{ref} = 120^\circ$, Re = 186, We = 11.4, Fr = 75387, Bi = 0.000116, $Pe_F = 40$ and different solid phase Peclet numbers $Pe_S = 100$, $Pe_S = 200$ and $Pe_S = 400$ for both M1 and M2 contact angle models.

tal heat transfer from the solid substrate into the liquid droplet increases with a decrease in the Peclet number. Lower the Peclet number, greater is the thermal conductivity of the solid which results in a higher rate of the heat transfer from the solid substrate into the liquid droplet. In short, we can conclude that the effect of temperature-dependent contact angle decreases with an increase in the Peclet number.

5. Summary

The dynamic contact angle as a function of temperature-dependent surface tension and reference equilibrium contact angle is proposed for computations of non–isothermal liquid droplet impingement on a hot solid substrate. Further, a finite element scheme using the arbitrary Lagrangian–Eulerian approach for the simulations of a non–isothermal liquid droplet with the proposed dynamic contact angle is presented. An array of numerical simulations for different reference equilibrium contact angles, solid phase initial temperatures, Reynolds numbers, Weber numbers and Peclet numbers of solid phase are performed using the temperature-independent (M1) and the temperature-dependent (M2) contact angle models are performed. In all test cases, the wetting diameter, the dynamic contact angle and the total heat transfer from the solid substrate into the liquid droplet are analyzed. The following observations are made in this numerical study.

- Contact angle models M1 and M2 result in almost identical flow dynamics for partially wetting liquids ($\theta_e^{ref} < 90^\circ$).
- For highly wetting liquids ($\theta_e^{ref} << 90^\circ$), the effects of temperature-dependent contact angle on the flow dynamics of the droplet are clearly observed.
- In the case of non-wetting liquids ($\theta_e^{ref} > 90^\circ$), the effects of temperature-dependent contact angle on the flow dynamics are significant and as high as 10.79% on the wetting diameter and 7.32% on the total heat transferred from the solid substrate into the liquid droplet.
- The effects of temperature-dependent contact angle are visible and significant only when the surface force dominates.
- More effects of temperature-dependent contact angle could be observed for higher values of the rate of change of surface tension with respect to the temperature.
- In order to capture the flow dynamics of the droplet and to predict the total heat transfer from the solid into liquid phase accurately, the choice of temperature-dependent contact angle model is essential in non-wetting and highly wetting impinging droplet simulations.

References

Adamson, A.W., 1973. Potential distortion model for contact angle and spreading. ii. temperature dependent effects. Adv. Colloid Interface Sci. 44 (2), 273–281.
Behr, M., Abraham, F., 2002. Free-surface flow simulations in the presence of inclined walls. Comp. Methods App. Mech. Eng. 191 (47–48), 5467–5483.
Bernardin, J.D., Mudawar, I., Walsh, C.B., Franses, E.I., 1997. Contact angle temperature dependence for water droplets on practical aluminum surfaces. Int. J. Heat Mass Transfer 40 (5), 1017–1033.
Briones, A., Ervin, J.S., Putnam, S.A., Byrd, L.W., Gschwender, L., 2010. Micrometer–sized water droplet impingement dynamics and evaporation on a flat dry surface. Langmuir 26 (16), 13272–13286.
Chandra, S., di Marzo, M., Qiao, Y.M., Tartarini, P., 1996. Effect of liquid-solid contact angle on droplet evaporation. Fire Saf. J. 27, 141–158.
Cox, R.G., 1986. The dynamics of the spreading of liquids on a solid surface. part 1. viscous flow. J. Fluid Mech. 168, 169–194.
Dussan V, E.B., 1976. The moving contact line: the slip boundary condition. J. Fluid Mech. 77 (4), 665–684.
Eggers, J., Stone, H.A., 2004. Characteristic lengths at moving contact lines for a perfectly wetting fluid: the influence of speed on the dynamic contact angle. J. Fluid Mech. 505, 309–321.
Francois, M., Shyy, W., 2003. Computations of drop dynamics with the immersed boundary method, part 1: numerical algorithm and buoyancy-induced effect. Numer. Heat Transfer Part B 44 (2), 101–118.
Francois, M., Shyy, W., 2003. Computations of drop dynamics with the immersed boundary method, part 2: drop impact and heat transfer. Numer. Heat Transfer Part B 44 (2), 119–143.
Ganesan, S., 2013. On the dynamic contact angle in simulation of impinging droplets with sharp interface methods. Microfluid. Nanofluid. 14, 615–625.
Ganesan, S., 2015. Simulations of impinging droplets with surfactant-dependent dynamic contact angle. J. Comput. Phys. 301, 178–200.
Ganesan, S., Matthies, G., Tobiska, L., 2007. On spurious velocities in incompressible flow problems with interfaces. Comput. Methods Appl. Mech. Eng. 196 (7), 1193–1202.

Please cite this article as: J. Venkatesan et al., Effects of temperature-dependent contact angle on the flow dynamics of an impinging droplet on a hot solid substrate, International Journal of Heat and Fluid Flow (2016), http://dx.doi.org/10.1016/j.ijheatfluidflow.2016.10.003

Ganesan, S., Rajasekaran, S., Tobiska, L., 2014. Numerical modeling of the non–isothermal liquid droplet impact on a hot solid substrate. Int. J. Heat Mass Transfer 78, 670–687.
Ganesan, S., Tobiska, L., 2008. An accurate finite element scheme with moving meshes for computing 3D-axisymmetric interface flows. Int. J. Numer. Methods Fluids 57 (2), 119–138.
Ganesan, S., Venkatesan, J., Rajasekaran, S., 2015. Modeling of the non–isothermal liquid droplet impact on a heated solid substrate with heterogeneous wettability. Int. J. Heat Mass Transfer 88, 55–72.
Gennes, P.G.D., 1985. Wetting: statics and dynamics. Rev. Mod. Phys. 57, 827–863.
Ghafouri-Azar, R., Shakeri, S., Chandra, S., Mostaghimi, J., 2003. Interactions between molten metal droplets impinging on a solid surface. Int. J. Heat Mass Transfer 46 (8), 1395–1407.
Harvie, D.J.E., Fletcher, D.F., 2001. A hydrodynamic and thermodynamic simulation of droplet impacts on hot surfaces. part II: validation and applications. Int. J. Heat Mass Transfer 44 (14), 2643–2659.
Hocking, L.M., 1977. A moving fluid interface. part 2. the removal of the force singularity by a slip flow. J. Fluid Mech. 79 (2), 209–229.
M.-C. Lai, Y.-H. T., Huang, H., 2010. Numerical simulation of moving contact lines with surfactant by immersed boundary method. Commun. Comput. Phys. 8 (4), 735–757.
Neumann, A., 1974. Contact angles and their temperature dependence: thermodynamic status, measurement, interpretation and application. Adv. Colloid Interface Sci. 4 (2–3), 105–191.
Neumann, A., Haage, G., Renzow, D., 1971. The temperature dependence of contact angles polytetrafluoroethylene/n-alkanes. J. Colloid Interface Sci. 35 (2), 379–385.
Petke, F., Ray, B., 1969. Temperature dependence of contact angles of liquids on polymeric solids. J. Colloid Interface Sci. 31 (2), 216–227.
Putnam, S.A., Briones, A.M., Byrd, L.W., Ervin, J.S., Hanchak, M.S., White, A., Jones, J.G., 2012. Microdroplet evaporation on superheated surfaces. Int. J. Heat Mass Transfer 55 (21–22), 5793–5807.
Ren, W., Weinan E, 2007. Boundary conditions for the moving contact line problem. Phys. Fluids 19, 022101.
de Ruijter, M., Klsch, P., Vou, M., Coninck, J.D., Rabe, J., 1998. Effect of temperature on the dynamic contact angle. Colloids Surf. A 144 (2–3), 235–243.
Schonhorn, H., 1966. Dependence of contact angles on temperature: polar liquids on polypropylene. J.Phys. Chem. 70 (12), 4086–4087.
Shewchuk, J.R., 2002. Delaunay refinement algorithms for triangular mesh generation. Comput. Geom. 22 (1–3), 21–74.
Steinke, S.K.M., 2001. Contact angles of droplets during spread and recoil after impinging on a heated surface. Chem. Eng. Res. Des. 79 (4), 491–498.
Strotos, G., Gavaises, M., Theodorakakos, A., Bergeles, G., 2008. Numerical investigation of the cooling effectiveness of a droplet impinging on a heated surface. Int. J. Heat Mass Transfer 51 (19–20), 4728–4742.
Sui, Y., Ding, H., Spelt, P.D., 2014. Numerical simulations of flows with moving contact lines. Annu. Rev. Fluid Mech. 46, 97–119.
Turek, S., 1999. Efficient Solvers for Incompressible Flow Problems. An Algorithmic and Computational Approach. Springer-Verlag Berlin.
Venkatesan, J., Ganesan, S., 2015. On the Navier-slip boundary condition for computations of impinging droplets. In: 2015 IEEE 22nd International Conference on High Performance Computing Workshops, pp. 2–11. doi:10.1109/HiPCW.2015.10.
Y. Ge, L.S.F., 2005. Three-dimensional simulation of impingement of a liquid droplet on a flat surface in the Leidenfrost regime. Phys. Fluids 17, 027104.
Y. Ge, L.S.F., 2006. 3-D modeling of the dynamics and heat transfer characteristics of subcooled droplet impact on a surface with film boiling. Int. J. Heat Mass Transfer 49 (21–22), 4231–4249.
Zhao, J.F.Z., Poulikakos, D., 1996. Heat transfer and fluid dynamics during the collision of a liquid droplet on a substrate. 1. modeling. Int. J. Heat Mass Transfer 39 (13), 2771–2789.

Please cite this article as: J. Venkatesan et al., Effects of temperature-dependent contact angle on the flow dynamics of an impinging droplet on a hot solid substrate, International Journal of Heat and Fluid Flow (2016), http://dx.doi.org/10.1016/j.ijheatfluidflow.2016.10.003